Techno-economic performance optimization of hydrothermal doublet systems Application to the Al Wajh basin, Western Saudi Arabia

Ezekiel, Justin; Ebigbo, Anozie; Arifianto, Indra; Daniilidis, Alexandros; Finkbeiner, Thomas; Mai, P. Martin

DOI
10.1016/j.geothermics.2022.102532

Publication date
2022

Document Version
Final published version

Published in
Geothermics

Geothermics 105 (2022) 102532

Contents lists available at ScienceDirect

Geothermics

journal homepage: www.elsevier.com/locate/geothermics

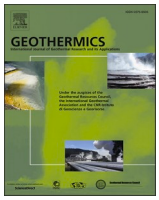

Techno-economic performance optimization of hydrothermal doublet systems: Application to the Al Wajh basin, Western Saudi Arabia

Justin Ezekiel [a,*], Anozie Ebigbo [b], Indra Arifianto [a], Alexandros Daniilidis [c], Thomas Finkbeiner [a], P. Martin Mai [a]

[a] Physical Science and Engineering Division, King Abdullah University of Science and Technology, Thuwal, 23955-6900, Saudi Arabia
[b] Hydromechanics Group, Helmut Schmidt University, Holstenhofweg 85, Hamburg 22043, Germany
[c] Faculty of Civil Engineering and Geoscience, Reservoir Engineering, Delft University of Technology, Stewinweg 1, Delft 2628CN, the Netherlands

ARTICLE INFO

Keywords:
Techno-economic optimization
Hydrothermal systems
Levelized cost of heating (LCOH)
Transmissivity
Thermoelastic fracture
Western Saudi Arabia

ABSTRACT

The Kingdom of Saudi Arabia (KSA) has vast geothermal energy resources. When developed, these markedly strengthen the country's goals of achieving a carbon-neutral economy. To demonstrate the feasibility and techno-economic performance of small-scale, hydrothermal well doublet systems for direct use in KSA, we perform reservoir and wellbore flow and heat-transport simulations as well as an economic analysis. The maximum permissible flowrate is constrained to avoid thermoelastic fracturing in the near-wellbore region. Reservoir conditions of a sedimentary basin along the Red Sea coast (near Al Wajh) provide an ideal study case to which we add economic parameters considered representative for KSA. We derive a Levelized Cost of Heat (LCOH) ranging from 49 to 128 $/MWh for 50-mD hydrothermal doublet systems with an optimal well spacing of 600 m and a flowrate ranging from 110 kg/s to 50 kg/s. LCOH is strongly influenced by decreasing reservoir transmissivity. Also, a minimum injection temperature is required to avoid thermoelastic fracturing. Our economic analysis further highlights that capacity factor and well-drilling cost have the greatest impact on LCOH. Thus, this study provides a guide and workflow to conduct techno-economic investigations for decision-making, risk mitigation, optimizing geothermal-energy-extraction and economic-performance conditions of hydrothermal doublet systems.

1. Introduction

One of the greatest socio-economic challenges of this century is how to provide energy to a growing global population while mitigating global climate change and achieving a decarbonized future. Carbon dioxide (CO_2) emissions related to energy consumption worldwide continue to increase despite temporary reductions related to the Covid-19 pandemic (Le Quéré et al., 2020; Liu et al., 2022). Geothermal energy is a promising renewable, sustainable, clean energy source that significantly contributes to solving the above challenge (Rybach, 2003; Axelsson et al., 2005). Geothermal energy becomes increasingly relevant in reducing CO_2 emissions, with installed capacity increasing worldwide (Lund and Toth, 2021; Tester et al., 2021). Over five years (2015–2020), the installed thermal power increased by 52% (at a compound rate growth of 8.7% annually) and the thermal energy used increased by 72% (at a compound rate growth of 11.5% annually) (Lund and Toth, 2021).

The economy of the Kingdom of Saudi Arabia (KSA) depends primarily on fossil fuels to meet energy and electricity demands (IEA, 2018), burning more oil directly for power generation than any other country and consuming 0.4–0.6 million barrels/day of oil to meet its electricity demand (EIA, 2020; Al Ghamdi, 2020). In addition, the rapid socio-economic growth in KSA increases the per capita water demand, stressing already limited freshwater supplies and making KSA the first country worldwide to require water desalination to meet potable water needs for domestic and industrial applications (Dawoud, 2005; ECRA, 2009). However, fossil-fuel-based energy supply to provide fresh water and space cooling to millions is unsustainable, cost-inefficient, and increases CO_2 emissions. CO_2 emissions from fossil-fuel-based electricity generation, massive desalination projects, and industrialization influence macro and microclimate changes. Greenhouse emissions are projected to further increase due to increases in (i) population, (ii) the use of air-conditioning in energy-inefficient buildings, and (iii) freshwater

Abbreviations: AW, Al Wajh; AWSO-1, Al Wajh South 1; KSA, Kingdom of Saudi Arabia; U.S., United States; TF, thermoelastic fracture; UL, Umm Lujj.

* Corresponding author.
E-mail address: chima.ezekiel@kaust.edu.sa (J. Ezekiel).

https://doi.org/10.1016/j.geothermics.2022.102532
Received 5 May 2022; Received in revised form 27 June 2022; Accepted 23 July 2022
Available online 30 July 2022

Nomenclature

Dimensionless parameters and constants

α	sensitivity term
η	pump efficiency
σ_{eff}	minimum effective hoop stress
μ	coefficient of sliding friction
ν	Poisson's ratio
CoP	coefficient of performance
CF	capacity factor
dT	thermal breakthrough (decay)
n_w	number of wells drilled

Variables

c	cost contingency (%)
CapEx_t	capital expenditure in year t ($)
C_{ex}	exploration cost ($)
C_w	well drilling cost ($)
dP	injection-induced pressure buildup at the injection well (Pa)
E	Young's modulus (Pa)
E_p	electricity price for pumping ($/W-hr)
GG	geothermal gradient (°C/km)
h_{inj}	enthalpy of the injected fluid (J/kg)
h_{wh}	enthalpy of the fluid at the production wellhead (J/kg)
LCOH	levelized cost of heat ($/MWh)
L_p	length of pipeline (m)
P_{th}	average thermal power (W_{th})
P_{th_t}	thermal power generated in year t (W_{th})
$\dot{m}$	mass flowrate (kg/s)
m_0	base-case LCOH performance metrics
m_{high}	+15% deviation of the LCOH performance metrics from the base case
m_{low}	–15% deviation of the LCOH performance metrics from the base case
n	project lifetime (years)
OpEx_t	operational expenditure in year t ($)
P_p	pore pressure (Pa)
P_{pump}	parasitic power used by the pump (W_{th})
P_{wh}	production wellhead pressure (Pa)
r	annual discount rate (%)
S_{hmin}	minimum principal horizontal stress (Pa)
S_{Hmax}	maximum principal horizontal stress (Pa)
t	production time (year)
T_0	initial reservoir temperature (°C)
T_{inj}	injection temperature (°C)
T_{prod}	downhole production temperature (°C)
T_{wh}	production wellhead temperature (°C)
Z	depth (m)
α_t	thermal expansion coefficient ($°C^{-1}$)
ΔP	pressure difference between the production and injection wellheads (Pa)
ΔT	wellbore cooling (°C)
ρ_f	fluid density (kg/m^3)
$\sigma^{\Delta T}$	thermal cooling stress (Pa)

demand for human consumption, agricultural and industrial activities (IEA, 2018; Almazroui, 2020). This unsustainable situation will worsen unless more vigorous climate-responsive actions and policies are adopted now and in the future.

To mitigate CO_2 emission, the government of KSA has initiated a nationwide circular carbon economy program to champion widespread use and upscaling of renewable energy sources (Al-Douri et al., 2019), and to develop advanced technologies that can reuse, remove and recycle emitted carbon. An energy-optimization study (Farnoosh et al., 2014) showed that by integrating fossil-fuel-based power and renewables in KSA, the country may save up to 28% of the cost of generating electricity per year, starting from 2030. In addition, action plans are in place in KSA to generate ~40 GWe of solar power by 2032 from concentrated solar plants (CSP) and solar photovoltaic (PV) with an investment of 109 billion USD (Ahmad and Ramana, 2014; Salam and Khan, 2018; Amran et al., 2020). However, geothermal energy has been neglected as additional sustainable source to complement, not compete with, energy supply from the other renewables invested in KSA.

Geothermal-based cooling and water-desalination applications on a national scale in KSA will not only lower carbon emissions, but also accelerate activities to reduce the country's dependence on non-renewable energy sources. Geothermal energy offers many advantages compared to other forms of renewable energy sources (such as solar PV, wind, hydropower), which include,

(i) Geothermal energy systems provide thermal energy suitable for a wide range of applications, including distributed heating and cooling of individual buildings, communities, and cities (Tester et al., 2021), as well as driving innovative water-desalination processes.
(ii) Land requirement and water requirement for geothermal energy systems are far less compared to solar PV and wind farms.
(iii) Geothermal power plants supply continuous, reliable baseload electricity without additional backup facilities.
(iv) Geothermal energy is not affected by weather and remains available throughout the year, unlike other sources of renewable energy (solar, wind, and hydropower).
(v) Geothermal reservoirs can be tailored to allow for simultaneous CO_2 storage and heat recovery from hot geological formations if CO_2 is used as subsurface working fluid (Randolph and Saar, 2011; Ezekiel et al., 2020).

Furthermore, during their envisioned life cycle, geothermal power plants produce far less CO_2 compared to the other renewable energy sources (World Nuclear Association (WNA), 2011; IPCC, 2012).

Previous geothermal studies in KSA primarily focused on assessing and exploring enhanced geothermal systems (EGS) in hot dry rocks (HDR) and hot wet granitic rocks (HWR) (Al-Dayel, 1988; Lashin and Al Arifi, 2012, 2014). EGS in KSA's volcanic provinces may potentially provide primary energy for electricity generation and direct applications when harnessed (Pruess, 2006, 2008; Zhang et al., 2014a, 2014b; Xu et al., 2015; Lu, 2018). However, EGS poses environmental problems, is expensive to develop, and prone to induced seismicity (Majer et al., 2007; Buijze et al., 2019). In contrast, hydrothermal resources in sedimentary basins are characterized by naturally higher pore space volumes and larger permeability that facilitate fluid flow and surface contact area for heat exchange (Limberger et al., 2018). In KSA, hydrothermal systems are expected to contain saline brines as energy carrier fluids, which possibly may be enriched in lithium as a potentially economically viable commodity (Sanjuan et al., 2016; Huang et al., 2021). Such systems may also utilize CO_2 as the heat extraction fluid, simultaneously storing CO_2 in the porous and permeable hydrothermal reservoirs (Randolph and Saar, 2011; Ezekiel et al., 2020). Several such sedimentary basins with viable hydrothermal reservoirs exist along the Red Sea coast of western Saudi Arabia (Hughes and Johnson, 2005) that can be exploited for geothermal direct use applications.

Currently, there are no published studies on the potential of geothermal extraction from deep hydrothermal reservoirs in the Red Sea

basin. Also, no studies exist on reservoir modeling and simulation techniques to assess reservoir and economic conditions in KSA in terms of feasibility and potential performance of geothermal systems for direct-use applications. However, to enable incorporating geothermal energy into the renewable-energy mix of KSA, it is essential to assess the potential and techno-economic performance of hydrothermal systems under varying reservoir and economic conditions. Therefore, we conduct techno-economic performance-based parametric study of the hydrothermal systems using generic models with doublet well patterns. We aim to understand how variations in key reservoir parameters and optimization of controllable design and operational parameters influence the performance of the hydrothermal doublet system. We apply the insights gained to perform techno-economic modeling analyses of optimized hydrothermal doublet systems for a major syn-rift sedimentary basin at the Red Sea coast, the Al Wajh basin.

The Al Wajh basin is located in the North-Central part of the Red Sea basin (Fig. 1). We choose this study area for several reasons. First, the economic development and tourism projects planned for this region will lead to high local demands for electricity, heating, cooling, and water desalination. Second, government regulation requires the implementation of low-carbon energy. Third, some subsurface data are publicly available and provide information for our modeling. Fourth, the clastic sedimentary formations with suitable porosity and permeability in this basin are at depths adequate for geothermal energy extraction and utilization, including carbon storage.

In this study, we perform coupled reservoir and wellbore flow and heat-transport simulations of geothermal energy extraction as well as an economic analysis for generic and site-specific hydrothermal doublet systems. Considered reservoir parameters include geothermal gradient and reservoir depth; design and operational parameters are well spacing and circulation flowrate. For performance quantification, we define several metrics, namely (i) average production temperature and thermal power, (ii) the thermal breakthrough time (for reservoir heat depletion), (iii) the coefficient of performance (CoP; ratio of the thermal power generated to used pump power), and (iv) the techno-economic performance of the hydrothermal system (LCOH, Levelized Cost of Heat). Additional constraints are imposed on the system to prevent the adverse effect of excessive pressure buildup and thermoelastic fracture initiation at the injection well.

Considering two existing siliciclastic hydrothermal formations within the Al Wajh basin, with varying depths, thicknesses, and permeabilities, we investigate feasibility and techno-economic performance of potential hydrothermal doublet systems. We then compare our local study result to reported values for hydrothermal systems in the United States and Europe. Also, the sensitivity of economic parameters on the LCOH performance metric is investigated. The insights from our study serve as a guide for selecting suitable hydrothermal reservoirs and for improving their performance. In addition, our findings assist in decision-making for the optimal design and operation of a hydrothermal system (within the model's uncertainty and natural variability ranges) in sedimentary rift-basin in Saudi Arabia and in geologically similar regions of the world.

2. Target siliciclastic hydrothermal reservoirs along the Red Sea rift basin

From a publicly available report of the Al Wajh basin (Hughes and Johnson, 2005), we obtain (Fig. 2) a stratigraphic column based on an exploration well drilled by Saudi Aramco named Al Wajh South-1 (AWSO-1), located in the southern part of the basin. This well reaches

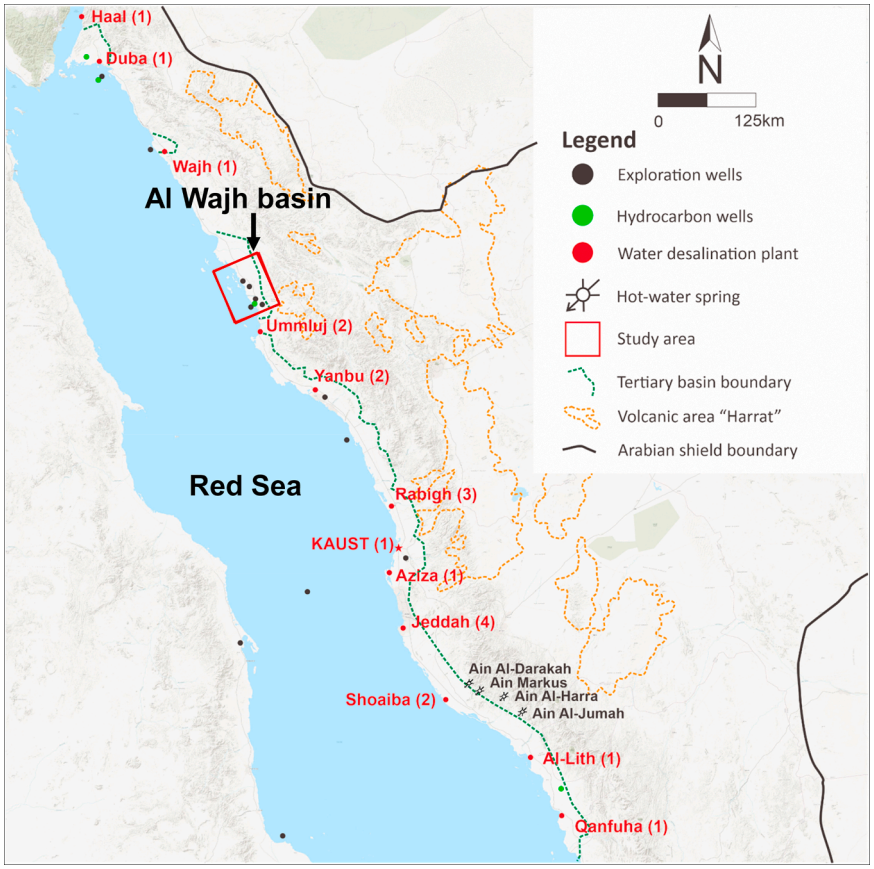

Fig. 1. Map showing the study area, the locations of exploratory wells, water desalination plants, sedimentary basins, and volcanic regions along the Red Sea rift (compiled from Girdler and Evans, 1977; Hughes and Johnson, 2005; Lashin and Al Arifi, 2014; Nada, 2013). The number of water desalination plants for each location is given in brackets.

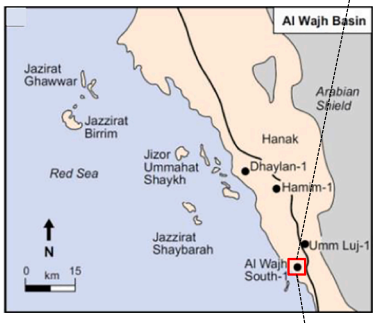

Extracted from Al Wahj South-1 (AWSO-1) Well, Al Wahj Basin, North Central Red Sea, Saudi Arabia								
Ma	Series		Group	Formation	Lithology	Depth (Fm base)	Calculated Temperature
1	Pleistocene		Quarternary sediments				
2–3	Pliocene	Late	Lisan Group				
4–5		Early					
6–9	Miocene	Late	Ghawwas Formation				
10–13		Middle	Mansiyah Formation		Evaporites (gypsum, anhydrite, halite)		
14			Maqna Group	Kial Formation	Interbedded anhydrites, mudstones, siltstone, hypersaline	1930 m	88 °C
15				Jabal Kibrit Formation	Coarse-grained siliciclastic facies of Umm Luj Member	2880 m	116.5 °C
16–17			Burqan Formation		Submarine fan sandsatones of Nutaysh Member	3820 m	145 °C
18–20		Early	Tayran Group	Yanbu Formation	Submarine evaporites (anhydrite, halite)	3900 m	147 °C
21–24				Al Wajh Formation	Marine siliciclastic	4100 m	153 °C
25–29	Oligocene	Late	Jizan Group	The Formations of the Suqah (Adaffa, Usfan, and Matiyah Formations) and Jizan Groups are missing in the Al Wahj South-1 well			
30–32		Middle	Suqah Group				
33–35		Early					
36–37	Eocene	Late					
49		Middle					
55		Early					
65	Paleocene						
Cretaceous							
Basement							

Fig. 2. Type section of the different Groups and Formations encountered by the Saudi Aramco exploration well Al Wajh South-1 (AWSO-1) well located in the Al Wajh basin, Red Sea rift. The lithology description, basal depths, and calculated temperatures (assuming a constant geothermal gradient of 30 °C/km and an annual mean surface temperature of 30°C) of the formations of interest are presented. Modified from Hughes and Johnson (2005).

a maximum (reported) depth of 4100 m TVD (Fig. 2).

The hydrothermal-reservoir-bearing strata in the study area suitable for geothermal energy are within early syn-rift intervals consisting primarily of sandstone and sandy conglomerate – namely Al Wajh Formation (Fm), Nutaysh Member of Burqan Fm, and Umm Lujj Member of Jabal Kibrit Fm (Fig. 2). These formations are thick (200–950 m), deeply buried (i.e., at 2–4 km depth) at sufficient temperatures (Fig. 2), possess good reservoir properties (Cole et al., 1995; Hughes and Johnson, 2005), and are unconformably embedded between low-permeability rock evaporitic formations acting as seals (Fig. 2) (Hughes and Johnson, 2005). The average reservoir porosity of the Burqan Fm is 22%, with an average permeability reaching 2 Darcy, while the porosity of the Jabal Kibrit and Al Wajh formations is up to 36%; determined from samples taken in the AWSO-1 well (Hughes and Johnson, 2005; Abdullatif and Osman, 2019).

This study only considers the Al Wajh and Umm Lujj reservoir units for our analysis (see Section 4.3). Due to the divergent plate-boundary Red Sea rifting, the study area has a relatively high heat flow (Girdler, 1970; Girdler and Evans, 1977; Pollack et al., 1993; Rolandone et al., 2013; Limberger et al., 2018). The Red Sea basin has a heat flux ranging from 70–90 mW/m^2 (Limberger et al., 2018; Lucazeau, 2019) with the Al Wajh basin (the focus area for this this study) up to 90 mW/m^2 near the town of Umm Lujj. This is significantly above the continental area average of 65 mW/m^2 (Pollack et al., 1993). The geothermal favorability map for KSA as created by Aboud et al. (2021), classifies the Al Wajh basin as a high to very high geothermal-favorable area.

3. Methods

In the following, we summarize our numerical modeling approach that evaluates reservoir performance and well configurations for hydrothermal doublet systems. Performance evaluation metrics and thermoelastic fracture initiation models provide the basis for a quantitative techno-economic evaluation of such systems. The results are presented and discussed in Section 4.

3.1. Hydrothermal reservoir model

As a base case, we set up a conceptual small-scale model of a horizontal, homogeneous hydrothermal reservoir (Fig. 3). The model is scalable for actual reservoir sizes, energy-potential, and energy-extraction schemes. The hydrothermal reservoir consists of a sandstone unit bounded by impermeable bedrock and caprock formations (e.g., evaporites), as present in the Al Wajh basin (see AWSO-1 well, Fig. 2). The area is 2×2 km^2, with a sedimentary layer thickness of 200 m and a permeability of 5×10^{-14} m^2 for the base case. These values are chosen to be the conservative reservoir-property averages of the hydrothermal system in the Al Wajh basin.

Further, we assume a doublet well pattern, consisting of a vertical injection well and a vertical production well. The wells are located near the center of the model and penetrate the entire hydrothermal reservoir. The computational grid is refined near the production and injection wells, and coarsens at the lateral boundaries to ensure both numerical accuracy and runtime efficiency. The grid-cell sizes range from $10 \times 10 \times 20$ m^3 to $50 \times 50 \times 20$ m^3.

As reservoir simulator, we use TOUGH2 (Pruess et al., 2012) including the module EWASG (Equation-of-State for Water, Salt, and Gas) (Battistelli et al., 1997). TOUGH2-EWASG allows to model geothermal reservoirs with three-component mixtures of water, sodium chloride (NaCl), and a slightly soluble non-condensable gas. TOUGH2 solves the fluid flow and heat transport equations, using the integral finite difference method for space discretization and the first-order, fully implicit, backward finite difference method for time discretization (Pruess et al., 2012). Dirichlet boundary conditions are set for the lateral boundaries of the reservoir pressure and temperature. There is heat flux, but no vertical fluid flow, from the reservoir to the overlying and underlying low-permeability formations. An initial steady-state model simulation defines the model's initial temperature and pressure fields.

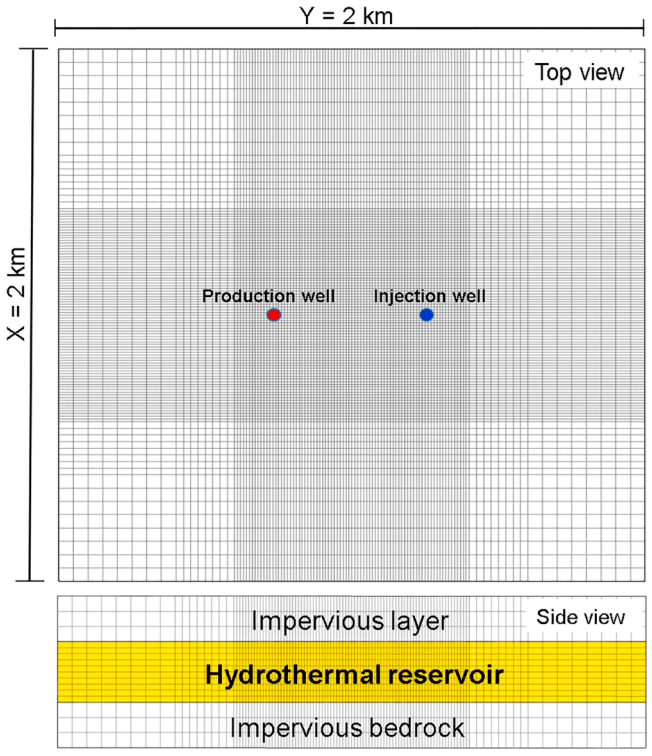

Fig. 3. Top and side views of the reservoir model showing the model's dimensions (2×2 km^2), the location of the production and injection wells, and the meshing. The side view shows a cross-section of the reservoir which has a thickness of 200 m and is bounded at the top and bottom by impervious layers that allow conducitve heat transfer but no fluid flow.

Temperature and pressure in the reservoir range from 100 °C and 23 MPa at the bottom to 105 °C and 25 MPa at the top of the reservoir as the initial conditions. The reservoir initially contains 20 wt% NaCl-brine.

3.2. Production wellbore and power-system model

Fluid pressure is expected to drop in the wellbore during production, depending on wellbore diameter, flowrate, friction, and other factors. A pump supports the fluid pressure at an appropriate depth to ensure production continues. Hence, it is vital to study all thermophysical processes at play during the entire production process.

We use an one-dimensional production wellbore model (Ezekiel et al., 2020, 2022). At any given time during simulated production, the initial conditions are defined as the reservoir (bottom-hole) pressure and temperature. The vertical production well is set up by dividing the depth to the reservoir top into 100 equal-sized elements. In the base case, the reservoir is at a depth of 2500 m, and the well is divided into 25 m-long vertical segments. Conservation of mass, as defined in (Adams et al., 2015; Ezekiel et al., 2022), is used to calculate the fluid state in the production well across each vertical well segment as the fluid flows up along the wellbore. We use CoolProp (Bell et al., 2014; CoolProp, 2019) for the iterative calculation of thermodynamic fluid properties, including the standard equations of state (Bell and Jäger, 2016). We adopt the assumption on production well material and hence its frictional properties, following (Ezekiel et al., 2020, 2022). The wellbore diameter is set to 0.315 m, similar to an average well diameter in geothermal fluid production (Bush and Siega, 2010). For simplicity, the wellbore model does not account for conductive and convective heat transfer to and from the rock in the near-wellbore region as the geothermal fluid is produced. Neglecting heat transfer in our wellbore model would lead to an overestimation of the wellhead temperature ranging from~0.5% for the shallow (low-temperature) to~2% for the deep (high-temperature) hydrothermal reservoirs.

The wellbore model is coupled with the (bottom-hole) reservoir simulation results to obtain the production wellhead temperature,T_{wh} and the wellhead pressure,P_{wh} of the produced fluid (as a function of time).T_{wh} andP_{wh} are used to calculate the enthalpy of the produced fluid at the production wellhead,h_{wh} (Eq. (1)), which is used to estimate the average thermal power (P_{th}) that can be generated at the surface (Eq. (2)).

$$h_{wh} = f(T_{wh}, P_{wh}) \tag{1}$$

$$P_{th} = \dot{m} \times \left(h_{wh} - h_{inj}\right) \times \text{CF} \tag{2}$$

In Eq. (2),$\dot{m}$ is the mass flowrate,h_{inj} is the enthalpy of the injected brine set in TOUGH2 (calculated using the injection temperature and the reservoir pressure) andCF is the capacity factor. We assume an average CF of 80%, which is within the typical values for geothermal operations (IEA Geothermal, 2017; EIA, 2019). The impact of the capacity factor to the economic viability of hydrothermal doublet systems are analysed in Section 4.5. The mass flowrate is equal for both the injection and production wells.

3.3. Simulation schemes

3.3.1. Hydrothermal doublet (base-case) model

Using the base-case parameters in Table 1, we set up a hydrothermal doublet (reservoir and wellbore) model (described in Section 3.1). Brine is circulated across the entire reservoir section at a pre-determined flowrate optimized to ensure sufficient power output and no excessive pressure buildup near the injection well. We investigate the effect of well spacing on the hydrothermal doublet system's thermal power output and overall performance. We assume well spacings between 200 and 800 m. Numerical boundary effects become apparent when the well spacing exceeds 800 m. In Section 4.1, we determine an optimal well

Table 1
Parameters used.

Reservoir Parameters: Varied	
Depth (km) *	1.5, 2.5, 3.5, or 4.5
Geothermal gradient (°C/km) *	20, 30, 40 or 50
Thickness (m) **	200 or 400
Permeability (m^2) **	1×10^{-14} to 2×10^{-13} (10–200 mD)
Reservoir Parameters: Not Varied	
Ambient mean surface temperature	30
Rock density (kg/m^3)	2600
Specific heat capacity (J/kg/°C)	1000
Effective thermal conductivity (W/m/°C)	2.1
Porosity (-)	0.2
Reservoir fluid	Brine (20 wt% NaCl)
Boundary conditions	Open (constant pressure and temperature)
Operational Design Parameters	
Well pipe diameter (m)	0.315
Fluid circulation rate (kg/s)	optimal (40 kg/s for base case)
Well spacing (m) ***	200 to 800
Injection temperature (°C)	52.50†
Production time (years)	40

* The base-case values for the thickness, reservoir permeability, and permeability anisotropy are 200 m, 5×10^{-14} m^2 and 1.0. The other values mentioned for the reservoir thickness and permeability are used to indicate and discuss variability in the case study section.

** The base-case values for the reservoir depth and geothermal gradient are 2.5 km and 30 °C/km.

*** Well spacing of 200–800 m is used only for the base-case simulations presented in Section 4.1. The well spacing of 400–700 m is used for the simulations of varying key reservoir parameters to reduce the number of simulations needed but still capture the effects of varying the well spacing.

† The injection temperature is estimated based on an annual mean surface temperature (30 °C) and an injection wellbore model.

spacing for the base-case hydrothermal doublet system. Re-injected brine temperature is 52.50 °C. Finally, we consider a simulated production period of 40 years, which is a reasonable lifespan for geothermal power plants (Adams et al., 2021).

3.3.2. Performance metrics

The important performance evaluation metrics for the hydrothermal doublet system are average reservoir production temperature, thermal power, thermal breakthrough time, the coefficient of performance (CoP), and the Levelized cost of heat (LCOH). These performance metrics are defined as follows:

(a) The average reservoir production temperature,T, and thermal power,P_{th}, can be used to identify hydrothermal doublet systems that show no thermal breakthrough but are unattractive due to their low production temperature and power generated.

(b) Thermal breakthrough time, expressed in years, is when the cold front connects to the production well. Thermal breakthrough is non-dimensional as a temperature fraction,dT, and expressed in Eq. (3).T_0 is the initial reservoir temperature,T_{prod} is the downhole production well temperature at time$t$, andT_{inj} is the injection temperature. We refer to thermal breakthrough time as the time,t_{TB} when dT declines by 5% from its original value at$t = 0$.

$$\mathrm{dT}(t) = T_0 - T_{\text{prod}}(t)/T_0 - T_{\text{inj}} \tag{3}$$

This performance metric can be used to determine the economically viable lifetime of the hydrothermal doublet system. Early thermal breakthrough leads to a decrease in the system's overall performance.

(a) The CoP (Eq. (3)) is a dimensionless (pressure-related) parameter to access the technical feasibility of the system (Ke et al., 2022). It considers the required parasitic pump power,P_{pump} (Eq. (4)). The higher the CoP, the better the performance of the hydrothermal doublet system.

$$CoP = P_{th}/P_{\text{pump}} \tag{4}$$

$$P_{\text{pump}} = (\dot{m} \times \rho_f \times \Delta P)/\eta \tag{5}$$

In Eq. (5),ΔP is the difference between the pressures at the production wellhead (calculated from the wellbore model) and the injection wellhead (taken as atmospheric pressure (Daniilidis et al., 2021)). Where applicable, we include in the numerator of Eq. (5) any extra pressure added to the system to ensure that pressure at the production wellhead remains above atmospheric pressure at all times.ρ_f andη are the density of the produced fluid and pump efficiency, respectively. We choose a pump efficiency of 75% (Menon, 2011).

(a) A geothermal system's economics can be evaluated by its Levelized Cost of Heat (LCOH) – a measure of the cost of (directly) using the extracted geothermal energy for any surface direct application. We calculate the LCOH using (Daniilidis et al., 2017), where LCOH over the project lifetime,$n = 40$ years, is defined as

$$LCOH = \frac{\sum_{t=1}^{n} \frac{CapEx_t + OpEx_t}{(1+r)^t}}{\sum_{t=1}^{n} \frac{P_{th_t}}{(1+r)^t}} \tag{6}$$

In Eq. (6),CapEx_t andOpEx_t are Capital and Operational expenses, respectively (in years t), r is the discount rate, andP_{th_t} is the thermal power generated in year$t$. In this study, the LCOH is calculated for annual and equally spaced timesteps of the modeled process. The reported LCOH values are the respective values at$t = 40$ years. We define CapEx as discrete investments, including the costs of drilling the wells (Lukawski et al., 2014; Daniilidis et al., 2017) (Eq. (7)), the costs for the exploration phase (DOE, 2016; Beckers and McCabe, 2019) (Eq. (8)), the construction costs (Eq. (9)) for the heat network facilities (DOE, 2016; Beckers and McCabe, 2019), and the recurring costs for the submersible pump (Daniilidis et al., 2021). A cost contingency factor c of 15%, covering equipment and miscellaneous expenses, is added to the CapEx (DOE, 2016; Beckers and McCabe, 2019). The total Operational Expenses (OpEx) is the sum of the fixed OpEx and the variable OpEx, whereby fixed Operational Expenses are calculated as a percentage of the CapEx, i.e., 5% per year. The cost of buying the pump electricity needed (for every operational hour) is calculated as the variable OpEx, as shown in Eq. (10) (Daniilidis et al., 2021),

$$C_w = 1.72 \times (0.2 \times Z^2 + 700 \times Z + 25000) \times (1+c) \times 1.184 \tag{7}$$

$$C_{ex} = 0.6 \times C_w + 10^6 + 0.12 \times (0.6 \times C_w + 10^6) \tag{8}$$

$$C_{gs} = (750 \times n_w \times 500) + (750 \times L_p) \tag{9}$$

$$\text{Variable OpEx} = P_{\text{pump}} \times E_p \times t \text{ (hour)} \tag{10}$$

Furthermore, we vary six economic parameters in a fixed range of±15% compared to their base-case values (Table 2) to investigate the corresponding sensitivity of the LCOH performance metric. The economic parameters include (i) calculated cost of drilling the wells, (ii) length of the pipeline to the gathering system, (iii) cost of pumps, and the number of times pumps need to be replaced during the system's lifetime, (iv) fixed OpEx (as a percentage of the CapEx), (v) electricity

Table 2
Economic parameters.

Capital investment (CAPEX)	
Drilled depth, Z (m)	according to the simulation scenario (2500 m base case)
Number of wells drilled, n_w (-)	2
Length of pipeline to the gathering system*, L_p (m)	1000
Cost of a well*, C_w ($)	See Eq. (7)
Cost of exploration, C_{ex} ($)	See Eq. (8)
Cost of gathering system, C_{gs} ($)	See Eq. (9)
Cost of a pump*, C_p (10^5 $)	5.90† (Daniilidis et al., 2021)
Cost contingency*, c (%)	15
Number of pumps used*, n_p (-)	2
Pump replacement interval*, t_{rp} (years)	5
Operational expenditure (OPEX)	
Fixed OpEx* ($)	5% of the total CapEx per year
Variable OpEx ($)	See Eq. (10)
Electricity price*, E_p ($/W-hr)	108.90† (Daniilidis et al., 2021)
Well spacing (m)	400 to 700
Annual discount rate, r (%)	7

* The sensitivity of these parameters on the LCOH performance metric is investigated (See Section 4.5).
† 2021 average foreign exchange rate of €1 = $1.184.

costs for pump operations, and (vi) percentage of cost contingency. The results (upper and lower bounds) of the LCOH for each of the respective parameter spaces were compared to the base-case LCOH.

We apply the method of (Ezekiel et al., 2021) to calculate the sensitivity,α, on the LCOH performance metrics (m) for±15% variations in the values of the economic parameters with respect to the base case, mathematically represented as (Eq. (11)),

$$\alpha = 33.33 \cdot \frac{m_{\text{high}} - m_{\text{low}}}{m_0} \tag{11}$$

The subscripts "high" and "low" denote the respective upper and lower bounds of the 15% deviation of the LCOH performance metrics from that of the base case (m_0). We present the economic parametric sensitivity results in Section 4.5.

3.3.3. Effects of reservoir and operational design parameters on hydrothermal doublet performance

We investigate the hydrothermal doublet system's sustainable performance using reservoir-parameter values of well AWSO-1 (Table 1). We vary reservoir depths from 1500 to 4500 m and geothermal gradients from 20 °C/km to 50 °C/km. The model is re-initialized for each new parameter set. The operational parameter well spacing (400–700 m) is varied to determine a performance-optimized well spacing. Then the model's optimized well spacing and pre-determined optimal flowrate (based on the highest flowrate for maximum admissible pressure buildup of 3 MPa at the injection well) are used to determine the effects of reservoir parameter variations on the techno-economic performance. This analysis helps to understand the reservoir-parameter sensitivity for the Al Wajh case study (see Section 4.3).

3.3.4. Thermoelastic fracture initiation model

Thermoelastic fracture (TF) initiation at the injection well has adverse effects on reservoir use. Therefore, we assess the possibility of initiating thermal-stress-induced fracture(s) in the injection well's reservoir interval. This evaluation is necessary to determine optimal hydrothermal doublet system design and operational parameters, and to avoid thermoelastic fracturing at the injection well. With the TF model, we restrict flowrates and pressure buildup to permissible values that prevent hydraulic fracturing.

Thermoelastic fracture initiation is evaluated by calculating the minimum effective hoop stress (σ_{eff}) at the injection wellbore wall (Eq. (12)) (Zoback et al., 2003). The calculatedσ_{eff} needs to stay above zero (assuming a conservative value for tensile strength, $T_0 = 0$ MPa) to avoid thermoelastic fractures. Following (Zoback et al., 2003),σ_{eff} is given as

$$\sigma_{\text{eff}} = \left(3S_{\text{hmin}} - 2S_{\text{Hmax}} - P_p - dP - \sigma^{\Delta T}\right) \rangle 0 \tag{12}$$

where,

$$S_{\text{hmin}} = \frac{S_{\text{v}} + P_p(f(\mu) - 1)}{f(\mu)} \tag{13}$$

S_{hmin} and S_{Hmax} are the far-field minimum and maximum principal horizontal stresses, respectively;P_p anddP are the pore pressure and the injection-induced pressure increase at the injection well, respectively. For a normal faulting environment, as expected for the Al Wajh basin,$S_V > S_{\text{Hmax}} > S_{\text{hmin}}$, where$S_{\text{hmin}}$ is constrained by Eq. (13). For our base case, we assume S_{Hmax} is the average betweenS_{hmin} and S_V.S_V is the vertical and greatest principal stress, here assumed to follow a gradient of 23 MPa/km Zoback et al., 2003). In the ensuing sensitivity analysis, we account for the following two SH_{max} uncertainty cases: (i) $S_{\text{Hmax}} = 1.1 \times S_{\text{hmin}}$ and (ii) $S_{\text{Hmax}} = 0.9 \times S_V$. In Eq. (13),$\mu$ is the coefficient of sliding friction generally ranging between 0.6 and 1.0 (Byerlee, 1978; Zaal et al., 2021). For simplicity, we consider the lower bound value of 0.6.$f(\mu)$ (Eqs. (13) and ((14)) is the function ofμ represented as,

$$f(\mu) = \left[\left(\mu^2 + 1\right)^{0.5} + \mu\right]^2 \tag{14}$$

The thermal cooling stress,$\sigma^{\Delta T}$ is calculated using Eq. (15) (Zoback et al., 2003).

$$\sigma^{\Delta T} = (\alpha_t E\ \Delta T)/(1 - \nu) \tag{15}$$

α_t is the thermal expansion coefficient, which is a strong function of silica content (Watanabe et al., 2004),ΔT is wellbore cooling, (difference between reservoir temperature and the injection temperature),E is Young's modulus andν is Poisson's ratio. The values of$E$ andν are chosen from their relationship with depth for sandstone (English, 2012).

4. Results and discussion

4.1. Performance of the (base-case) hydrothermal doublet reservoir

We investigate the performance of the base case hydrothermal system situated at a depth of 2500 m and a thickness of 200 m (Table 1) for varying well spacings (200–800 m) using the pre-determined optimal flowrate of 40 kg/s. Fig. 4a shows temperature depletion at the production well over time. Thermal breakthrough, (occurs for well spacings less than 600 m (larger distances are unaffected), with reservoir temperatures decreasing by 2–3% every five years for well spacings less than 500 m (Fig. 4).

Fig. 4b displays the performance metrics –T,P_{th}, CoP and LCOH, for the different well spacing. Due to the decreasing effect of thermal breakthrough for larger well spacings, T andP_{th} increases. However, at 500 m well spacing, their rates of increase slows down. For well spacings of 600 m and above, T remains the same due to no thermal breakthrough, whereasP_{th} and CoP decrease due to the increased pump power needed to compensate increasing pressure difference between production and injection well. The effect of reservoir impedance (due to increased reservoir space for fluid flow) becomes more significant for well spacing > 600 m leading to decreased CoP.

The CoP serves as preliminary parameter that indicates the start in performance decline of the hydrothermal doublet system. Also, LCOH decreases with increasing well spacing, down to a minimum of 156.20 $/MWh for a well spacing of 600 m. This indicates a 44% LCOH decrease for well spacings from 200 to 600 m. Between 600 m and 800 m spacing, LCOH gradually increases by 2%. Thus, the base-case simulation results suggest that a 600 m well spacing is optimal as it exhibits no thermal breakthrough over the system's 40-year lifespan and results in the highestP_{th} and CoP, and the lowest LCOH.

Furthermore, assuming a 100% capacity factor and 5% discount rate,

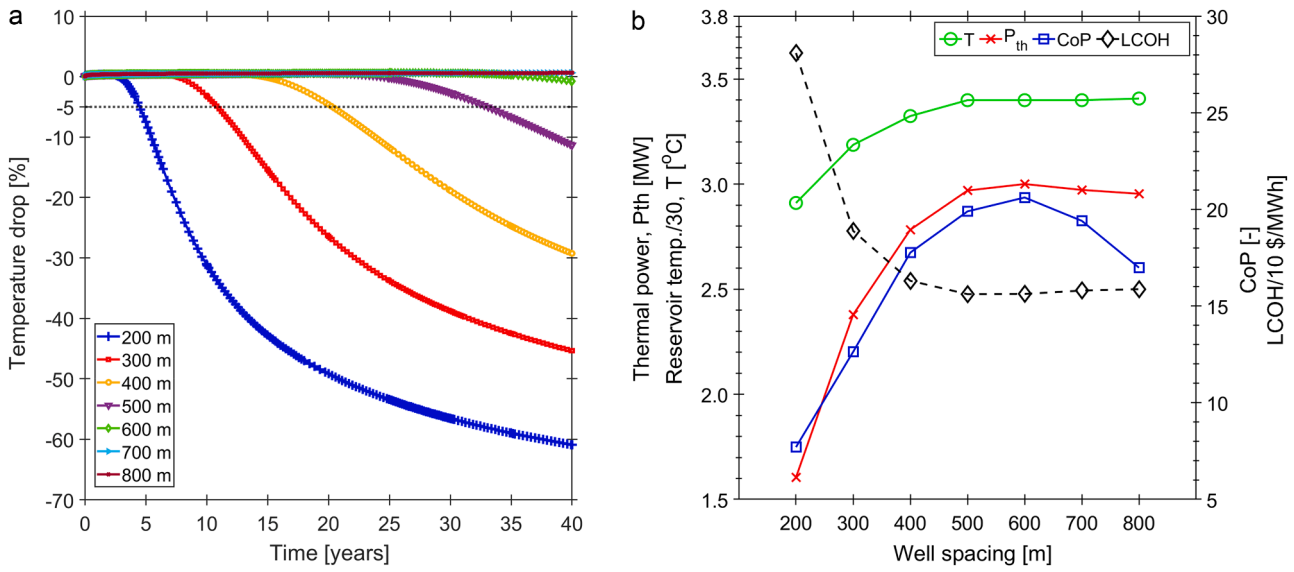

Fig. 4. (a) Temperature drop (expressed as a percentage decline in the original value of dT at $t = 0$) over time, and the equivalent reservoir production temperatur after 40 years, for well spacing of 200 m to 800 m. 5% indicates the start of thermal breakthrough. Thermal breakthrough and temperature drop are not observed for well spacing ≥ 600 m (the reservoir production temperature remains the same after 40 years), (b) Average reservoir production temperature, average thermal power, CoP and the LCOH over time for well spacing of 200 to 800 m. Optimal well spacing is determined to be 600 m.

the minimum LCOH value (at 600 m spacing) of 156.20 $/MWh is halved. This indicates the strong impact these two parameters would have on the economic feasibility (LCOH) of the hydrothermal doublet system. The effects of these parameters are discussed in detail in Section 4.5.

Fig. 5 displays the temperature distribution after 40 years (end of the simulation). The cold front reaches the production well if the well spacing equals or is less than 400 m. This result matches the thermal breakthrough pattern observed in Fig. 4a. The cold plume does not reach the production well for spacings of 600 m and above (Fig. 5).

4.2. *Effects of variation of key reservoir parameters on the performance metrics*

Next, we examine how geothermal gradient and reservoir depth variabilities affect the performance metrics – average production temperature and thermal power, thermal breakthrough time, CoP, and LCOH. Starting from a constant ambient surface temperature of 30 °C, we vary the geothermal gradient from 20 °C/km to 50 °C/km and reservoir depths from 1500 m to 4500 m (at a constant thickness of 200 m). These variations are expected to influence the geothermal system's performance directly. While reservoir depth and geothermal gradient are set by nature and cannot be influenced, we can optimize operational parameters such as well spacing. All other base-case reservoir parameters are kept constant (Table 1), and we again use the pre-determined optimal flowrate of 40 kg/s.

4.2.1. *Average production temperature, thermal power and thermal breakthrough time*

Tables 3a and b list increasing average production temperature and thermal power generated as reservoir depth and geothermal gradient increase. There is little effect on these two performance metrics with widening well spacing. Low production temperatures (<73 °C) estimated for shallow reservoir depth (1500 m) and geothermal gradients less than 40 °C /km generate negative power. Hence hydrothermal reservoirs with such low production temperatures may be not attractive or feasible for geothermal energy development. In contrast, for production temperatures above 80 °C, at least 1 MW_{th} average power can be generated.

An increase in the well spacing prolongs the thermal breakthrough time (Table 3c, Fig. 4a). Table 3c shows that for closer well spacings, thermal breakthrough occurs sooner as reservoir depth and geothermal gradient increase. This effect is caused by lower fluid density associated with higher volumetric flowrate. Interestingly, thermal breakthrough is

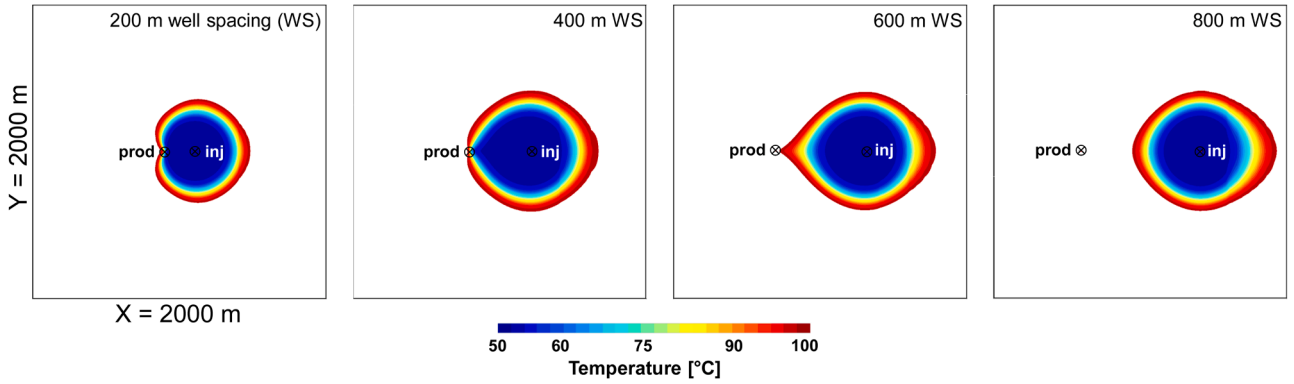

Fig. 5. Temperature distributions in aerial view for the base case after 40 years and doublet-well spacings (DS) of 200, 400, 600, and 800 m. No thermal breakthrough occurs at the production well when the well spacing is ≥600 m. Note that model sections with a temperature greater than 100 °C are blank.

Table 3
List of calculated average reservoir production temperatures (°C) (a), average thermal power (MW_{th}) (b), and thermal breakthrough times estimated in years (c) as a function of various geothermal gradients, reservoir depth, and increasing well spacing (from 400 to 700 m). There is no thermal breakthrough for well distances ≥ 600 m, as indicated by blank. Even though there is no thermal breakthrough for cases with average reservoir production temperature less than 73 °C (at well distances ≥ 600 m), they generate negative power (shown as blank cells in (b)). Hence, these low production temperature cases are not economically viable for development.

(a) Average reservoir production temperature (°C)

	20				30				40				50				GG* [°C/km]
Depth [m]	400	500	600	700	400	500	600	700	400	500	600	700	400	500	600	700	Spacing** [m]
1500	58	58	58	58	71	72	72	72	84	86	86	86	98	100	100	100	
2500	77	78	78	78	100	102	102	102	123	126	126	126	147	149	150	150	
3500	96	98	98	98	129	132	132	132	162	165	166	166	195	199	200	200	
4500	115	118	118	118	157	161	162	162	201	205	206	206	243	249	250	250	

(b) Average thermal power (MW_{th})

	20				30				40				50				GG [°C/km]
Depth [m]	400	500	600	700	400	500	600	700	400	500	600	700	400	500	600	700	Spacing [m]
1500									1.2	1.4	1.4	1.4	2.7	2.9	2.9	2.9	
2500	0.3	0.4	0.4	0.4	2.8	3	3	3	5.3	5.6	5.6	5.6	7.9	8.1	8.2	8.2	
3500	2.3	2.4	2.4	2.4	5.8	6.1	6.1	6.1	9.4	9.7	9.8	9.8	13	13.3	13.4	13.4	
4500	4.2	4.4	4.5	4.5	8.8	9.1	9.2	9.2	13.4	13.8	13.9	13.9	17.9	18.4	18.5	18.5	

(c) Thermal breakthrough times (year)

(c)	20				30				40				50				GG [°C/km]
Depth [m]	400	500	600	700	400	500	600	700	400	500	600	700	400	500	600	700	Spacing [m]
1500	20.5	33.1			19.9	31.9			20.3	33.1			20.6	33.3			
2500	20	32.5			20.5	33.1			21	34.1			21.5	34.9			
3500	20.3	33.2			21.2	34.4			21.7	35.2			22.1	35.7			
4500	21	34			21.7	35.2			22.2	35.9			22.3	36.1			

* GG stands for geothermal gradient.
** Well spacing starts from 400 m (instead of 200 m in Section 4.1) to reduce the number of simulations.

not reached for the shallowest reservoir depth and the 20 °C/km geothermal gradient, irrespective of well spacing. This is due to the low temperature difference between reservoir temperature (60 °C) and injection temperature (52.50 °C), resulting in slower migration of the dense (cold) injected fluid. However, if well spacing is less than 500 m, thermal breakthrough occurs in the shallowest reservoir case for the geothermal gradients greater than 20 °C/km. Recall that there is no thermal breakthrough for the optimal base-case well spacing (600 m) for all geothermal gradients and reservoir depths (Fig. 4).

Furthermore, cases with very low production temperature (resulting in negative power) may have no thermal breakthrough at well spacing≥600 m (Table 3c); however, their low production temperature still does not render them economically viable for development. In addition, low reservoir production temperature, with positive but low power, may also not be suitable for certain direct-use application (such as spacing cooling and industrial applications). This needs to be put into consideration per use case.

4.2.2. Coefficient of performance (CoP)

Using the CoP results for varying reservoir parameters, we determine the optimal well spacing. First, we define a dimensionless CoP fraction between 0 and 1, by dividing the CoP for each doublet spacing by the maximum CoP from all well spacing simulations. Fig. 6 shows the mean of all CoP fraction values for each well spacing. The top and bottom boundaries of the box represent the first (upper 25%) and the fourth (lower 25%) quartiles of the CoP fraction values, whiskers represent the minimum and the maximum CoP fractions. The doublet with well spacing of 600 m has mean CoP fraction closest to 1, shortest quartiles and whiskers, and hence is the optimal system's design in terms of well spacing.

Furthermore, the change in CoP fraction for 100 m increments in well spacing and related uncertainty in obtaining the optimal spacing is more pronounced for smaller well spacings (≤500 m). From the slope in CoP fraction in Fig. 6, we infer the energy penalty for choosing a sub-optimal well spacing. Too narrow well spacings incur a higher penalty than those that are too wide.

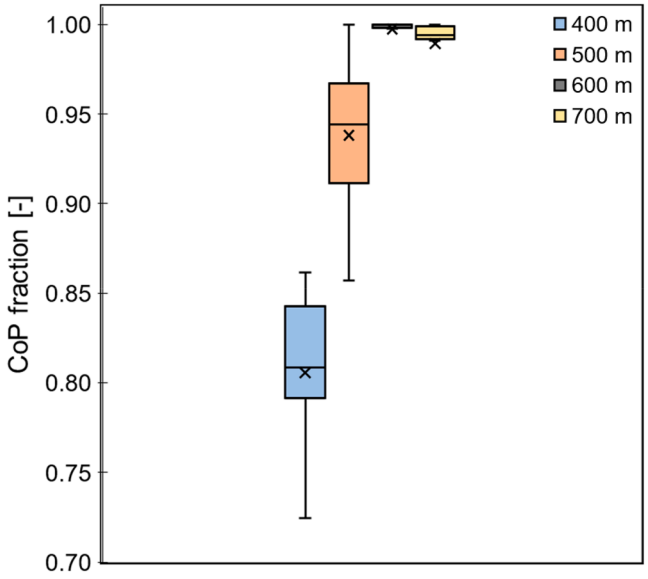

Fig. 6. Box and whisker plot showing the CoP fraction for various geothermal gradients and depth parameter spaces for well spacing of 400 m to 700 m. The 600 m well spacing achieves the maximum CoP fraction value.

Fig. 7 exhibits that the maximum CoP per 1-kilometer depth (ΔCoP_{max}/km) changes most rapidly between 1.5 km and 2.5 km, with 30 and 39 ΔCoP_{max}/km values for the GG cases of 40 °C/km and 50 °C/km, respectively.ΔCoP_{max}/km increases as the geothermal gradient increases due to the higher thermal power generated for the high geothermal gradients of 40 °C/km and 50 °C/km. However,ΔCoP_{max}/km decreases with depth because of increasing pump power requirement, slowing the rate CoP increases with depth. The drop in CoP for the 4500 m reservoir depth case when GG increases from 40 °C/km to 50 °C/km could result from the large increase in required pump power.

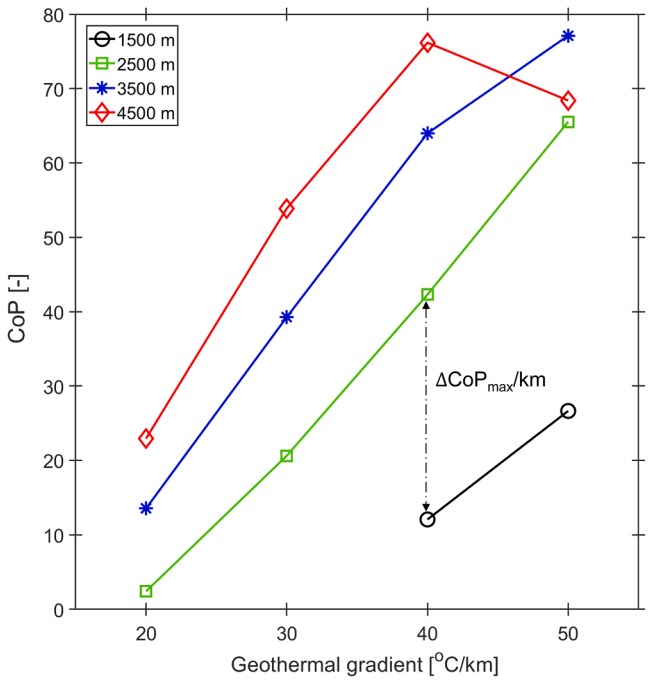

Fig. 7. Plot of maximum CoP vs. geothermal gradient for different depths, showing the change in maximum CoP per 1 km depth as geothermal gradient increases. The maximum CoP is at the 600 m well spacing.

To a lesser degree, this effect is also noticeable when the reservoir is 3500 m deep; CoP increases more slowly as GG increases from 40 °C/km to 50 °C/km.

4.2.3. Levelized cost of heating (LCOH)

The levelized cost of heating indicates the cost (in $/MWh) of extracting heat from the hydrothermal resources for direct-use purposes. As shown in Eq. (5), LCOH is a function of both the CapEx and OpEx divided by the amount of energy extracted and discounted by 7% in this case.

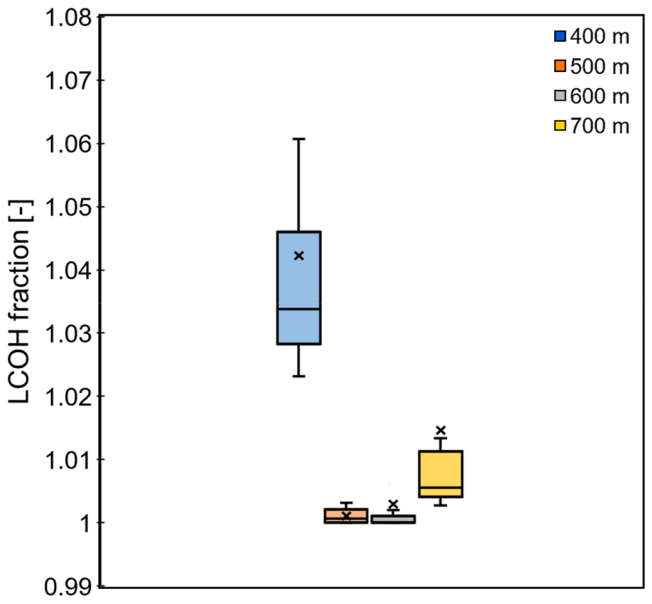

Fig. 8. Box and whisker plot showing the LCOH fraction for various geothermal gradients and depth parameter spaces for well spacing of 400–700 m. The lowest values of the LCOH fraction also correspond to the optimal 600 m well spacing.

Fig. 8 shows a box and whisker plot of the calculated LCOH fraction, derived by dividing the LCOH for each well spacing by the minimum LCOH value across all well spacing for the evaluated parameter ranges. LCOH fraction decreases as well spacing increases to 600 m, where LCOH exhibits a minimum. However, by further increasing well spacing to 700 m, the LCOH increases slightly. The increment in LCOH is due to increased pump power to compensate for larger pressure differences for widely spaced injection and production wells (spacing > 600 m). Hence, the increase in well spacing results in higher CoP and lower LCOH, but all optimal performances are at the 600 m well spacing for the hydrothermal system. Fig. 8 also shows that albeit well spacings of 500 m and 700 m have similar mean LCOH fractions, we expect the 500 m spacing to have better economic performance due to smaller error bands.

Using the optimal well spacing with lowest LCOH, Fig. 9 displays the LCOH results for varying geothermal gradients and depths. LCOH decreases as the geothermal gradient and depth increase. Hence, as the hydrothermal reservoir becomes hotter, there will be less cost (per MWh) for developing the hydrothermal doublet system.

For reservoir depths shallower than 3000 m, LCOH is high for geothermal gradients less than 30 °C/km (Fig. 9). In contrast, LCOH reduces markedly when the geothermal gradient increases above 30 °C/km. This indicates that a hydrothermal system at shallower depths will not be economically viable for heat extraction unless the geothermal gradient is moderately high (≥ 30 °C/km). For geothermal gradients above 40 °C/km, reservoirs above 3000 m depth have LCOH ranging from 80–210 $/MWh, while deeper reservoirs (i.e., below 3000 m) yield LCOH between 52 and 68 $/MWh. For a 2500 m deep reservoir (base case) and optimal well spacing of 600 m, Fig. 9 shows that LCOH drops from 1208 to 156 $/MWh (87% decrease) when the geothermal gradient increases from 20 °C/km to 30 °C/km. However, if the geothermal gradient increases from 30 °C/km to 40 °C/km, the LCOH drops to 83 $/MWh (47% decrease). It decreases further to 52 $/MWh (37% decrease) if the geothermal gradient increases from 40 °C/km to 50 °C/km. This suggests an asymptotic relationship between LCOH and an increase in geothermal gradient, depth, reservoir temperature, and

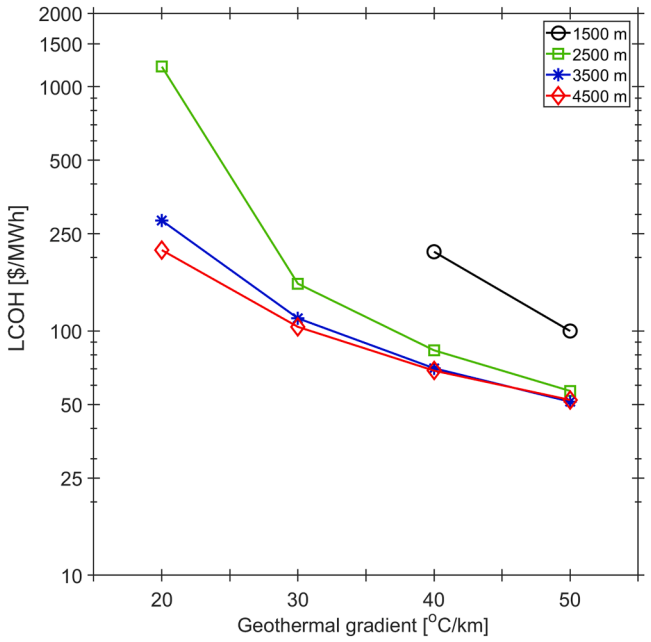

Fig. 9. Semilog plot of the minimum LCOH for varying geothermal gradients of 20–50 °C/km and reservoir depths ranging 1500–4500 m. LCOH decreases as the geothermal gradient and reservoir depth (i.e., temperature in general) increase. Negative power is generated for the 1500 m depth case at low/mid geothermal gradients of 20 °C/km and 30 °C/km. Hence they are omitted from the plot.

power generated (see Fig. 9). This implies that the expenditure, especially the cost of drilling to the deeper formations, leads to a decrease in the rate of LCOH drop as depth (and temperature) increase. The LCOH for the 40°C/km and 50°C/km geothermal gradients become equal at deeper depths of 3500 m and 4000 m.

4.3. Case study: modeling the techno-economic performance of the hydrothermal doublet system of the Al Wajh basin

As described in the Section 2, we use the Al Wajh Formation (Fm) considered to have favorable hydrothermal conditions (Fig. 2), as a case-study reservoir to investigate the techno-economic performance of geothermal energy development in the Red Sea region. Fig. 2 indicates that the AWSO-1 well only encountered the 200 m thick Al Wajh Formation at 4100 m. We use the small-scale reservoir model's dimensions (2 × 2 km) for the case-study simulations. The hydrothermal doublet system's optimal well spacing of 600 m is used. We assume an average surface ambient temperature of 30 °C (consistent with mean surface temperature for the region) and an average one-dimensional geothermal gradient of 30 °C/km. This results in a subsurface temperature of about 150 °C in the Al Wajh Formation. To accommodate the natural and uncertain permeability distribution, we set a range for the reservoir model from 10 mD to 200 mD with an average of 50 mD.

Furthermore, we compare the simulation results for the Al Wajh Formation to the Umm Lujj (UL) Member of the Jabal Kibrit Fm (depth of 2350 m) in the Al Wajh basin (Fig. 2). However, we now assume that the top 400 m section of the Umm Lujj Member (out of the 900 m thickness, Fig. 2, (Hughes and Johnson, 2005)) is the reservoir target of interest. This assumption enables us to compare two hydrothermal reservoirs in the Al Wajh sedimentary basin, with varying thicknesses (200 and 400 m) and depths (4100 and 2350 m). At constant geothermal and pressure gradients for the two target units, the shallower but thicker Umm Lujj Member will have lower reservoir production temperature (see Table 4 – Scenario A) and pressure than the deeper (but thinner) Al Wajh Formation.

In the techno-economic performance evaluation of the case-study hydrothermal doublet system, we first determine the optimal flowrate corresponding to an admissible pressure buildup of 3 MPa at the injection well. The downhole injection pressures do not exceed induced fracture initiation pressures at the wellbore wall and the pressure propagation away from the well. This is also needed to avoid inducing fractures or injection under fracturing conditions. Next, the LCOH is calculated using the corresponding thermal-power and pump-power simulation results. Note that the base-case injection temperature (52.50 °C) and the pre-determined optimal well spacing of 600 m (Section 4.2) are used.

Table 4 (Scenario A) summarizes the resulting performance metrics and average power generated for the Al Wajh Formation at varying permeability and transmissivity (a product of reservoir permeability and thickness (Birdsell et al., 2021)). The optimized flowrate increases with transmissivity, which increases the average thermal power and decreases the LCOH. The higher the flowrate and transmissivity, the better the performance of the hydrothermal doublet system. The LCOH values significantly decrease as permeability changes from 10 mD to 50 mD. This indicates that low-permeable reservoirs generate lower thermal power and require higher development costs. Note that the CoP decreases with increased transmissivity and flowrate due to the higher pump power required as flowrate increases.

Comparing the simulation results (Scenario A) of the 50-mD case of the deeper but thinner Al Wajh Fm to the 50-mD case of the shallower but thicker Umm Lujj Member, the optimal flowrate determined for the latter is 60 kg/s higher than the former (Table 4 – Scenario A). The higher flowrate results from the larger reservoir transmissivity of the Umm Lujj unit. However, the thermal power generated by the Al Wajh Fm (with lower flowrate) is higher than that of the Umm Lujj Member because of the higher temperature associated with deeper formation.

Table 4
Performance for the deep Al Wajh Fm case at varying reservoir permeability and the 50 mD case of the shallower Umm Lujj Member of the Jabal Kibrit Fm. Three scenarios are considered – Scenario A: using the base-case injection temperature of 52.50 °C. Scenario B: using the minimum injection temperature only without optimizing the flowrate to achieve 3 MPa pressure buildup (*dP*) at the injection well. The minimum injection temperature ensures that the undesirable thermoelastic fracture is not initiated at the injection well. Scenario C: using the minimum injection temperature and the corresponding re-optimized flowrate. Note that transmissivity (m^3) is calculated as a product of permeability and thickness.

Target Formations (Fm)	**Al Wajh Fm**				**Umm Lujj (Jabal K. Fm)**
Permeability (mD)	10	50	100	200	50
Transmissivity (10^{-12} m^3)	2	10	20	40	20
Scenario A – using the base-case injection temperature of 52.50°C					
Optimal flowrate (kg/s)	10	50	100	200	110
Maximum *dP* (MPa)	2.92	2.99	3.00	3.00	2.91
Ave. reservoir temperature (°C)	150	150	146	139	100
Ave. surface prod. temp. (°C)	144	144	141	134	97
Ave. thermal power (MW_{th})	1.88	9.33	18.16	32.68	7.58
CoP (-)	44.45	41.63	32.37	23.87	23.46
LCOH ($/MWh)	439.42	90.81	47.92	29.71	62.20
Scenario B – using the minimum injection temperature that will not induce TF*					
Min. inj. temperature (°C)	82	83	83	83	36 (no TF†)
Maximum *dP* (MPa)	2.02	1.91	1.86	1.79	
Ave. thermal power (MWth)	0.84	4.34	7.62	12.24	
CoP (-)	19.94	19.43	13.00	9.60	
LCOH ($/MWh)	984.34	195.59	108.61	73.73	
Scenario C – using the minimum injection temperature and the re-optimized flowrate**					
Re-optimized flowrate (kg/s)	15	81	160	325	100
Maximum *dP* (MPa)	3.00	3.00	2.93	2.94	3.00
Ave. surface prod. temp. (°C)	144	143	138	133	97
Ave. thermal power (MWth)	1.26	6.70	11.10	18.96	9.52
CoP (-)	17.52	14.40	10.10.	6.82	32.66
LCOH ($/MWh)	657.02	128.00	84.76	67.84□	48.71

* The simulations for Scenario A are carried out with the minimum injection temperature (to limit inducing TF) without re-optimizing the flowrate to match the 3-MPa permissible pressure buildup at the injection well.

** The simulations for Scenario B consider both minimum injection temperature (to limit inducing TF) and the re-optimized flowrate to match the 3-MPa permissible pressure buildup at the injection well.

† No TF will be initiated for the Umm Lujj case because the minimum injection temperature required for TF initiation (36°C) is less than the injection temperature (52.50 °C) used in this study. Hence there is no Scenario A for the Umm Lujj case.

□ For the highest transmissivity Al Wajh Fm case, the high flowrate leads to an early thermal breakthrough, and thus LCOH increases.

Interestingly, although the 50-mD Al Wajh Fm case has a higher thermal power output, the LCOH of the 50-mD Umm Lujj Member case is lower by 32%. This is because the overall cost of developing a deep and thinner Al Wajh Fm to generate 9.33 MW_{th} of power is significantly higher than the cost to develop a shallower reservoir with higher transmissivity and flowrate. Hence, if a good geothermal gradient (e.g., 30 °C/km) exists, it is economically more feasible to target high transmissivity reservoirs even if they are at moderate depths (> 2000 m).

Note that the thickness of Al Wajh may be larger than reported for the AWSO-1 well (Hughes and Johnson, 2005), for locations further north by tens of kilometers. In this case, the transmissivity of the Al Wajh Fm might be greater or equal to that of the Umm Lujj Member, making it

most likely that the Al Wajh Fm will have a lower LCOH than the Umm Lujj Member. Also, if the permeability of the hydrothermal reservoirs of the Al Wajh basin decreases with depth, the deep Al Wajh Fm's performance would worsen due to the expected increase in the LCOH values as reservoir permeability and transmissivity decrease (Table 4). However, when the transmissivity value for shallower and deeper reservoirs are equal, (e.g., the 100-mD Al Wajh Fm and the 50-mD Umm Lujj Member have identical transmissivity of 2×10^{-11} m^3) we observe that the deeper Al Wajh Fm performs better (Table 4 – Scenario A).

Our preliminary results show that our small-scale case-study model is highly scalable to achieve higher power output and reduce costs. Hence, our findings show that the proposed system is worth considering for real applications. It can be readily implemented in Red Sea sedimentary basins with deep hydrothermal reservoirs to produce significant energy for direct-use applications. In addition, we can achieve potential synergies if the two case-study hydrothermal formations are developed sequentially or simultaneously. The synergic benefits include (i) increasing the total producible geothermal energy due to higher produced geofluids and production temperature (Table 4 – Scenario A), which may meet the requirements for geothermal electric power generation; (ii) using the generated power (electric and/or thermal) to power operations of the Red Sea development project in the Al Wajh region, thereby increasing the energy system efficiency of the project; (iii) sharing existing infrastructure (surface facilities, wells, exploration costs, etc.) and jointly utilizing multidisciplinary datasets (on reservoir parameters), thereby reducing investment costs and hence LCOH significantly; (iv) extending the useful lifespan of the geothermal field, thereby postponing the decommissioning of the field and reusing otherwise stranded assets.

4.4. Performance evaluation considering thermoelastic fracture initiation

To further evaluate the performance of the hydrothermal doublet system, we derive limits for the injection pressure to avoid hydraulic fracturing. As presented in Section 3.3.4, induced fractures initiate when the hoop stress around the wellbore wall reaches the tensile strength of the surrounding rock. This pressure limit is influenced by principal stress differences and thermal effects – the difference between the reservoir and fluid injection temperatures. At a fixed flowrate, a higher injection temperature reduces the chances of TF occurring. Hence, optimizing the system using a minimum injection temperature and an optimized flowrate that limits TF initiation is important. For the assumed permeability range of Al Wajh Fm (Table 4), using the base-case injection temperature of 52.50 °C, the high difference between injection and reservoir temperature would initiate TF at the injection well. This is true because deeper reservoirs with high temperatures require higher injection temperatures to avoid thermoelastic fracture initiation. From Table 4, our simulations show that the minimum injection temperature to prevent TF initiation is about 82–83 °C for all permeability cases. Since the Umm Lujj Member is at a shallower depth, the temperature difference is low and would not induce TF. Hence, there is no Scenario B for the Umm Lujj Member case, however, its minimum injection temperature should stay above 36 °C.

To prevent hydraulic fracturing, we consider two scenarios (B and C) for optimizing the performance of the hydrothermal doublet systems in the Al Wajh basin. Scenario B considers the pressure-buildup-related optimized flowrate (obtained in Scenario A) and the minimum injection temperature obtained for each case (Table 4 – Scenario B). The simulation results reveal that pressure build up at the injection well reduces to 1.86–2 MPa when assuming minimum injection temperature. We can further optimize the system by increasing the flowrate until pressure buildup at the injection reaches ~3 MPa. In Scenario C, we optimize the system by using the re-optimized (increased) flowrate and the minimum injection temperature. Hence, Scenario B considers TF optimization based on injection temperature correction only, while Scenario C considers re-optimized flowrate and the injection temperature adjustments.

For Scenario B, LCOH further increases by 2–3 times as transmissivity decreases for the Al Wajh Fm cases. However, assuming a higher flowrate, LCOH does not increase for Scenario C as much as it increases for Scenario B. Hence, to avoid TF initiation, injection temperature and flowrate need to be re-optimized to improve the economic feasibility of the system. Fig. 10 (Scenarios B and C) shows an increased LCOH after 10–15 years of production for high transmissivity 200 mD of the Al Wajh Fm in response to rapid thermal breakthrough and a decrease in CoP due to high flowrate (i.e., 325 kg/s). The LCOH calculations terminated at 36 years because production temperatures dropped below the minimum injection temperature. Thus, flowrate optimization for high transmissivity hydrothermal doublet systems should be constrained by both pressure build-up and thermal breakthrough.

For the Umm Lujj case (Scenario C), we reduce the excess injection temperature (52.50 °C) to match the minimum injection of 36 °C. When the flowrate is re-optimized, it drops from 110 kg/s to 100 kg/s. However, a better LCOH (by 22%) is achieved when reducing the injection temperature to its estimated minimum. Thus, it is crucial to evaluate the minimum injection temperature and the associated optimal flowrate for the hydrothermal system to avoid hydraulic fracturing of the injection well.

With the limited data available at the time of this study, the magnitude of S_{Hmax} is highly uncertain. Within this normal faulting environment, S_{Hmax} may range from close to S_{hmin} (i.e., $S_V > S_{Hmax} \sim S_{hmin}$) to close to S_V (i.e., $S_V \sim S_{Hmax} > S_{hmin}$). Thus, we conduct an uncertainty analysis to understand its impact on LCOH. The results suggest that when S_{Hmax} is close to the S_{hmin} (i.e., $S_{Hmax} = 1.1 S_{hmin}$), there is a favorable decrease in the LCOH for the Al Wajh hydrothermal doublet system. The decrease in LCOH is due to the reduction in the minimum injection temperature from about 83 °C (Table 4) to 38 °C, which leads to a 38 $/MWh and 41 $/MWh decrease in LCOH for the 50 mD and 100 mD permeability cases of Al Wajh, respectively. The Umm Lujj Member is not considered in this lower-bound variation of S_{Hmax}, because it is already at a suitable low minimum injection temperature (36 °C) for the base-case value of S_{Hmax}. In the other extreme, however, when S_{Hmax} is close to S_V (i.e., $S_{Hmax} = 0.9 S_V$), the minimum injection temperatures required to avoid hydraulic fracturing of the Al Wajh Fm and Umm Lujj Member are very high (i.e., 125 °C and 83 °C, respectively). These values are close to the initial temperatures of the reservoirs (153 °C and 98 °C, respectively). This implies that the operations of the case-study hydrothermal doublet systems may not be feasible for such a high value of S_{Hmax}.

The simulation results indicate the importance of conducting a detailed geomechanical study for the geothermal systems to robustly constrain stress magnitudes, in particular S_{Hmax}, to avoid hydraulic fracturing and other production problems, and thereby incorrectly estimating LCOH (Table 4, Fig. 10 – Scenarios B and C). In addition, it would be important to couple geomechanical processes with fluid-rock chemical interactions to calculate a minimum injection temperature threshold to avoid scaling and mineral precipitation around the wellbore region.

4.5. Sensitivity of the economic parameters on the LCOH

As illustrated in Section 3.3.2, we evaluate the sensitivity of the economic parameters on the LCOH performance metric. The results are shown in Fig. 11, where we vary the economic parameters in a fixed range of ±15% compared to the base-case reservoir (see Section 4.1) and operational conditions (at constant 40 kg/s flowrate and 600 m well spacing for a 50-mD permeability and 200-m thick reservoir). The positive sensitivity value ($+\alpha$) seen for all the parameters (Fig. 11), except capacity factor, shows that an increase in the economic parameters' values will increase the LCOH and vice versa. The negative sensitivity value ($-\alpha$) seen for capacity indicate that an increase in the capacity

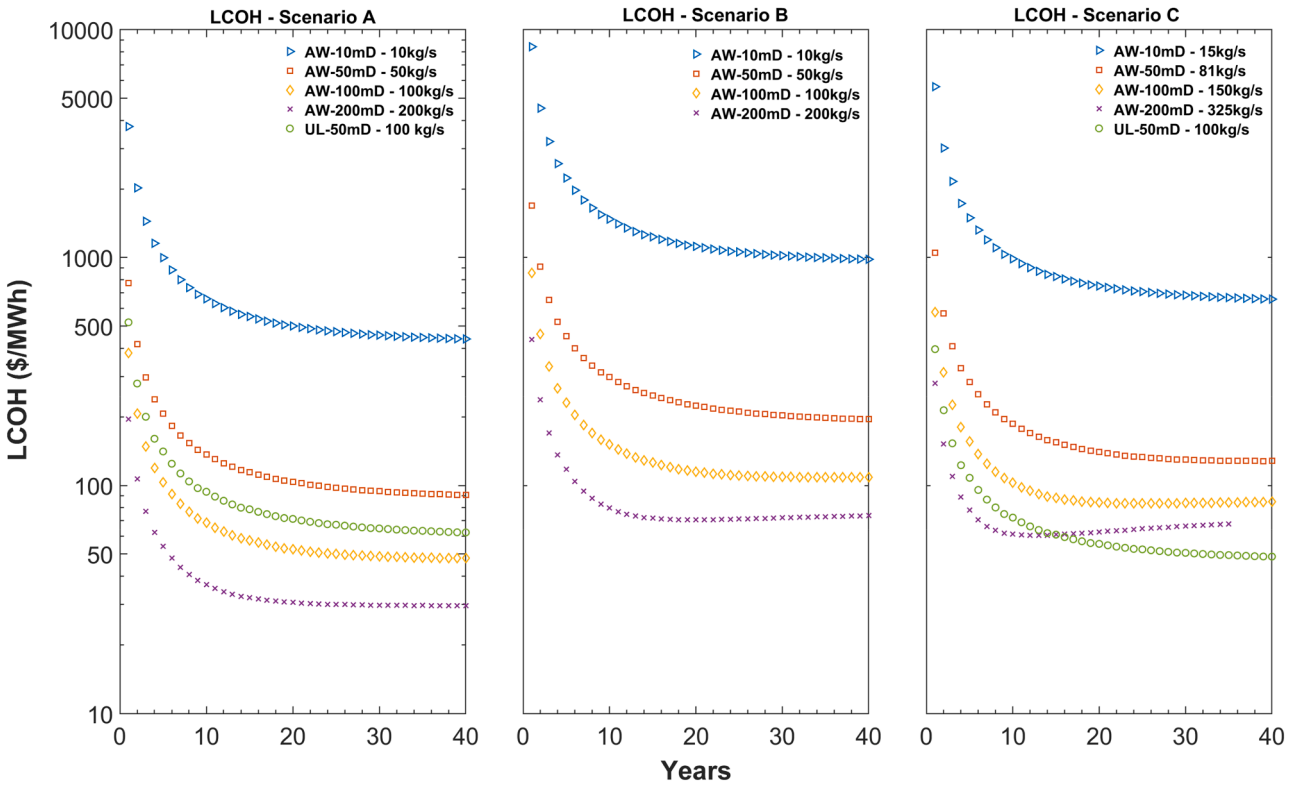

Fig. 10. LCOH versus time semilog plot for the scenarios A through C and varying permeability and corresponding optimized flowrate for the Al Wajh (AW) Fm and Umm Lujj (UL) Member hydrothermal doublet systems. LCOH for the 200-mD AW case in Scenario C stopped after 38 years due to fast thermal breakthrough.

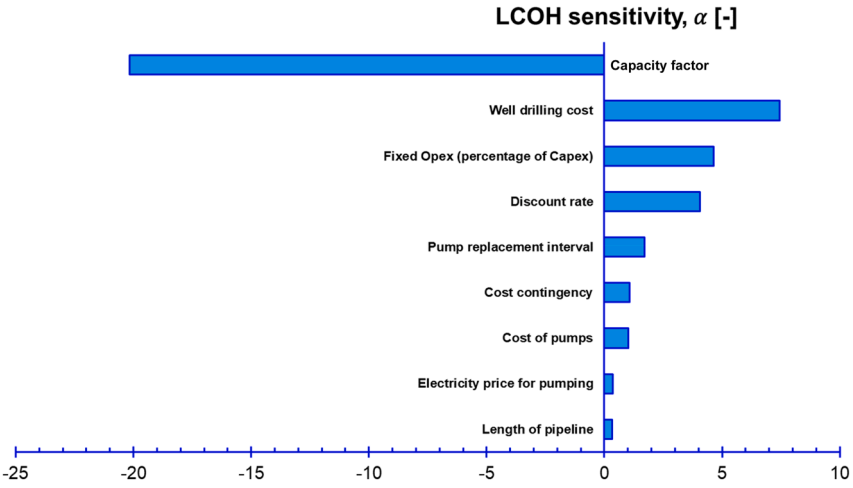

Fig. 11. Sensitivity of economic parameters on the LCOH (showing the most sensitive parameter (top) to the least sensitive parameter (bottom)). The positive (right-hand) part signifies that an increase in the parameter values will increase LCOH. The negative (left-hand) part identifies parameters that, when being increased, will result in a decrease in LCOH.

factor will decrease the LCOH and vice versa.

The sensitivity analysis (Fig. 11) shows that the capacity factor has the highest impact on LCOH. A 15% change in value of capacity factor will result to$\alpha = -21$, which implies a slight increase in capacity factor generally leads to a substantial reduction of the project's LCOH. For the parameters that show $+\alpha$, a 15% change to the base-case cost of drilling the two wells ($\alpha > +7.5$) and a 15% change in the fixed OpEx ($\alpha > +5$) are the parameters the LCOH is most sensitive to. The cost of exploration is proportional to the cost of drilling the wells, which is expected to drive the CapEx higher if there is an increase in drilling costs. They are followed by the discount rate ($\alpha > +4$). However, the sensitivity (in magnitude) of the capacity factor is about 4–5 times greater than these 3 parameters with positiveα.

The time interval for pump exchange is more sensitive to LCOH than the costs of the pumps. LCOH is not very sensitive to the change in electricity price used for pumping (Fig. 11). This indicates that a slight drop in CoP (due to higher pump power) will not significantly increase LCOH. Of all the parameters considered, LCOH is least sensitive to the change in pipeline length.

This initial economic sensitivity study is vital in determining factors that influence the LCOH, assuming the selected economic parameter values listed in Table 2 strongly differs from the economic conditions in

Saudi Arabia.

Typical geothermal power plants have a capacity factor less than 100% due to system downtime for maintenance or due to seasonal demand for heating and cooling buildings. However, higher capacity factors are seen for most industrial direct use where geothermal energy could provide the baseload power. In Western Saudi Arabia, the likely (impactful) direct use of geothermal energy is for district cooling and geothermal-based water desalination. Due to the hot weather conditions and scarcity of fresh water, these two direct applications of geothermal energy could be operational throughout the entire year, and there is no or minimal seasonal load factor reduction. Technical system maintenance has little effect on capacity if there is demand for the generated thermal power. Hence, capacity factor for geothermal systems could be assumed to be high (above 90%) for the case study of the Al Wajh basin. In this context, if the capacity factor increases from the base case value of 80% to 95%, the LCOH (Table 4 – Scenario A) decreases from 439 $/MWh to 312 $/MWh (a 29% decrease) for the lowest transmissivity case, and decreases from 29.7 $/MWh to 22.5 $/MWh (a 24% decrease) for the highest transmissivity case. Hence increasing capacity factor is immensely pertinent for improving performance and economic feasibility of the hydrothermal doublet system.

McCabe et al. (2019) listed eight parameters, grouped into three categories, which have the most significant impact on LCOH. The three categories and eight parameters include 1. Geothermal reservoir system - geothermal gradient, drilling capital cost (a function of reservoir depth and technological advancement), well flow rate, reservoir lifetime; 2. User application - surface equipment capital costs, reinjection temperature, and equipment lifetime; and 3. Financing - discount rate. The parameters reservoir lifetime and equipment lifetime can be referred to as system lifetime. A sensitivity study (Reber, 2013) shows that the geothermal gradient has the strongest impact on LCOH, but the geothermal gradient is controlled by nature and cannot be modified by technological advancements (McCabe et al., 2019). Aside from geothermal gradient, the three parameters of high impact on LCOH are drilling capital cost, well flowrate, and discount rate. Unlike geothermal gradient, these three parameters can be modified through technology improvements to reduce LCOH.

In Saudi Arabia, the cost of drilling and completing a well is relatively high. It could range from an estimated $2.5–3.5 million per km, depending on the type of well, scope, and location of the project. As shown in our economic model, well drilling costs affect other costs such as fixed OpEx (Eq. (9)) (Daniilidis et al., 2021) and cost of exploration (Eq. (7)) (DOE, 2016; Beckers and McCabe, 2019). Thus, any slight increase in drilling cost increases the overall LCOH. For example, from the economic model (see Section 3.3.2), the costs of drilling the well doublet for the 50-mD permeability cases of the (deep) Al Wajh Fm and the (shallower) Umm Lujj Member are about $12.75 million per well and $5.65 million per well, respectively. In other words, drilling costs may range from 12% to 16% of the total expenses for the two projects. The well drilling costs of four similar geothermal deep direct use projects in the United States (U.S.), where drilling costs ranges from 13 to 17% of the total project expenses (Beckers et al., 2021). Hence, a decrease in the drilling costs reduces the overall LCOH.

The parameter well flowrate can be optimized to achieve the best possible techno-economic performance for specific hydrothermal systems. A higher flowrate (under safe and controlled geomechanical conditions) will increase extracted thermal energy, thereby significantly reducing the LCOH. Proper reservoir design and management, coupled with good reservoir transmissivity, will allow for high flowrate and reduced project LCOH (Section 4.3 and Table 4).

Lastly, any reduction in discount rate decreases the LCOH. For example, a 15% decrease in discount rate of the 50-mD permeability cases of the (deep) Al Wajh Fm and the (shallower) Umm Lujj Member hydrothermal systems will result in a 5% and 4.2% decrease in LCOH, respectively. The discount rate can be reduced by de-risking the project, such as resource exploration and shifting the project from private/local interest to a large-scale government, institutional, or community interest (McCabe et al., 2019). Hence, this will lead to lower interest rates and increase the pay-back time of the borrowed funds.

More power will be generated at a smaller cost when upscaling the system by drilling more wells to extract more geothermal energy from the hydrothermal system. We remark that investment and operational costs decrease after successful drilling of the first set of well(s), due to increased data, information and knowledge that help reduce uncertainties and risks, and due to shared surface and drilling infrastructures.

4.6. A comparison of our LCOH results with other reported LCOH values of hydrothermal systems

A notable example of a hydrothermal doublet simulation is the Geothermal Electricity Technology Evaluation Model (GETEM) conducted using the GEOPHIRES v2.0 – a geothermal techno-economic simulation tool (Beckers and McCabe, 2019). The GETEM (Example 1 in (Beckers and McCabe, 2019)) comprises a 200-m thick, 100-mD permeability hydrothermal reservoir at 2000 m depth with average reservoir temperature of 120 °C. A doublet well configuration, with 900-m well spacing and 50 kg/s water production flowrate, and 80 °C injection temperature, is used. At a capacity (utilization) factor of 90%, the average thermal power generated for direct-use heat by the GETEM model is 7.2 MW_{th}. This value is similar to the average thermal power generated by the Umm Lujj case study (Table 4), therefore, we compare the GETEM's model to the Umm Lujj case study. The LCOH for our case study (using a capacity factor of 90%) is 39 $/MWh and 50 $/MWh, respectively with and without TF consideration. These LCOH values are comparable with the 32 $/MWh LCOH for the GETEM model, showing that the LCOH for our two case-study hydrothermal reservoirs are realistic.

Furthermore, we compare our LCOH for the considered hydrothermal doublet systems with actual and simulated LCOH for hydrothermal systems in the U.S. and Europe (McCabe et al., 2019). The simulated LCOH (including TF initiation modeling) for the 50-mD permeability cases of the shallow Umm Lujj Member and the deep Al Wajh Formation, of 49 $/MWh and 128 $/MWh, respectively, falls on the middle to lower-end range of estimated LCOH for geothermal district heating (GDH) systems in the U.S., estimated to 30–120 $/MWh (Thorsteinsson and Tester, 2010), and in Europe (Ungemach, 2012; Dumas and Angelino, 2015) (including France (Services and Ross Offshore, 2016), Italy (GeoDH, 2015a), Poland (GeoDH, 2015b), Slovenia (Kralj, 2005; GeoDH, 2015c), and Iceland (Petursson, 2015)), estimated to 21–85 $/MWh (Dumas and Angelino, 2015). These LCOH are comparable to the simulated LCOH for our case-study hydrothermal doublet systems.

Given the assumptions in our study, these comparisons indicates that the two hydrothermal systems (Al Wajh Fm and the Umm Lujj unit) could be high-performing hydrothermal systems. Thus, we conclude that the direct-use geothermal development in the Al Wajh basin (Western Saudi Arabia) is feasible under optimized operational conditions within the model's uncertainty and natural variability ranges.

5. Conclusion

We present a coupled reservoir-wellbore flow and heat-transport model, with the maximum permissible flowrate constrained to avoid thermoelastic fracturing in the near-wellbore region. The model is used to evaluate and optimize the techno-economic performances of generic and site-specific (Al Wajh basin, Western Saudi Arabia) small-scale hydrothermal doublet systems for direct-use applications. We define the following performance metrics: (i) average reservoir production temperature and average thermal power, (ii) thermal breakthrough time (reservoir heat depletion), (iii) Coefficient of Performance (CoP; ratio of thermal power generated to pump power used), and (iv) Levelized Cost of Heat (LCOH). Our sensitivity study examines how variations in key

reservoir parameters impact these performance metrics, and provides a quantitative tool to optimize design and operational parameters.

Our key findings include:

(1) The optimal well spacing with the highest techno-economic performance can be determined for hydrothermal doublet systems using the performance metrics. The performance metrics can also inform of the penalties incurred (in terms of lesser energy recovery and higher LCOH values) and illustrate that undersized well spacing is more costly as compared to oversized well spacing.
(2) The rate of change of the maximum CoP per kilometer (ΔCoP_{max}/km) increases as the geothermal gradient increases. However,ΔCoP_{max}/km decreases with depth (at a constant geothermal gradient) due to increasing pump power. Our simulation results show an asymptotic decrease in LCOH as geothermal gradient and depth increase. Hence, as the hydrothermal system gets hotter, development becomes cheaper (per MWh).
(3) Optimized flowrate increases with transmissivity for both the deeper but thinner Al Wajh Fm (permeability ranging from 10 mD to 200 mD) and the shallower but thicker 50-mD Umm Lujj Member; this increases the average thermal power generated whilst LCOH decreases. Correspondingly, CoP decreases with increasing transmissivity and flowrate due to the higher required pump power.
(4) LCOH varies from 49 to 128 $/MWh (at a capacity factor of 80%) for both the higher transmissivity 50-mD Umm Lujj Member and the lower transmissivity 50-mD Al Wajh Fm. However, when transmissivity for both hydrothermal systems are identical (equal transmissivity of 2×10^{-11} m^3 for 100-mD Al Wajh Fm and 50-mD Umm Lujj Member), the deeper Al Wajh Fm achieves the better overall performance.
(5) Determining the minimum injection temperature is critical to avoid thermoelastic fracturing (TF) in the injection well. Geothermal studies rarely account for geomechanical implications when injecting cold fluids and associated risks for hydraulic fracturing. This can lead to undesired production problems (e.g., injected fluids do not flow where expected). We further note that increasing injection temperature (to avoid TF), leads to an increase in LCOH. However, the flowrate should be optimized to improve system economics and ensure accurate estimation of optimal performance.
(6) A 15% change in capacity factor, drilling cost and fixed OpEx have the greatest impact on LCOH. A change in the pipeline length to transport produced geofluids to the use area has the least economic impact on the system.
(7) The LCOH range derived for the hydrothermal doublet systems in Al Wajh are comparable to those reported for existing hydrothermal systems in the U.S. and Europe. Hence, our techno-economic results show that the geothermal energy extraction from the proposed hydrothermal doublet system is feasible and should be further explored. We propose that such systems can be readily implemented in Red Sea sedimentary basins with deep hydrothermal reservoirs for geothermal energy direct-use applications. In addition, the small-scale hydrothermal doublet systems considered in this study is scalable by increasing the reservoir size and number of wells.

This study serves as a guide for identifying favourable reservoir factors for selecting suitable hydrothermal reservoirs in sedimentary rift-basin in Saudi Arabia and geologically similar regions of the world, and optimizing their operational design and techno-economic performances.

CRediT authorship contribution statement

Justin Ezekiel: Conceptualization, Methodology, Software, Formal analysis, Investigation, Resources, Data curation, Writing – original draft, Writing – review & editing, Visualization. **Anozie Ebigbo:** Conceptualization, Methodology, Formal analysis, Writing – review & editing. **Indra Arifianto:** Methodology, Software, Formal analysis, Investigation, Data curation, Visualization. **Alexandros Daniilidis:** Conceptualization, Methodology, Formal analysis, Writing – review & editing. **Thomas Finkbeiner:** Conceptualization, Methodology, Formal analysis, Resources, Writing – review & editing. **P. Martin Mai:** Conceptualization, Formal analysis, Resources, Writing – review & editing.

Declaration of Competing Interest

The authors declare that they have no known competing financial interests or personal relationships that could have appeared to influence the work reported in this paper.

Acknowledgments

The research presented in this paper is supported by King Abdullah University of Science and Technology (KAUST) in Thuwal, Saudi Arabia (grants BAS/1339-01-01, BAS/1/1421-01-01, and REI/1/4502-01-01 for JE, IA, PMM).

References

Abdullatif, O., Osman, M., 2019. Reservoir heterogeneity and quality of wajh formation: outcrop analog study, Red Sea region, Saudi Arabia. In: Proceedings of the 81st EAGE Conference and Exhibition. https://doi.org/10.3997/2214-4609.201901468.

Aboud, E., Qaddah, A., Harbi, H., Alqahtani, F., 2021. Geothermal resources database in Saudi Arabia (GRDiSA): GIS model and geothermal favorability map. Arab. J. Geosci. 14, 112. https://doi.org/10.1007/s12517-020-06426-z.

Adams, B.M., Kuehn, T.H., Bielicki, J.M., Randolph, J.B., Saar, M.O., 2015. A comparison of electric power output of CO_2 plume geothermal (CPG) and brine geothermal systems for varying reservoir conditions. Appl. Energy 140, 365–377. https://doi.org/10.1016/J.APENERGY.2014.11.043.

Adams, B.M., Vogler, D., Kuehn, T.H., Bielicki, J.M., Garapati, N., Saar, M.O., 2021. Heat depletion in sedimentary basins and its effect on the design and electric power output of CO_2 plume geothermal (CPG) systems. Renew. Energy 172, 1393–1403. https://doi.org/10.1016/j.renene.2020.11.145.

Ahmad, A., Ramana, M.V, 2014. Too costly to matter: economics of nuclear power for Saudi Arabia. Energy 69, 682–694. https://doi.org/10.1016/j.energy.2014.03.064.

AlGhamdi, A. 2020. Saudi Arabia Energy Report. King Abdullah Petroleum Studies and Research Center (KAPSARC) KS 2020 DP25. https://www.kapsarc.org/research/publications/saudi-arabia-energy-report/.

Al-Dayel, M., 1988. Geothermal resources in Saudi Arabia. Geothermics 17, 465–476. https://doi.org/10.1016/0375-6505(88)90076-4.

Al-Douri, Y., Waheeb, S.A., Voon, C.H., 2019. Review of the renewable energy outlook in Saudi Arabia. J. Renew. Sustain. Energy 11. https://doi.org/10.1063/1.5058184.

Almazroui, M., 2020. Changes in temperature trends and extremes over Saudi Arabia for the period 1978–2019. Adv. Meteorol. 2020, 8828421 https://doi.org/10.1155/2020/8828421.

Amran, Y.H.A., Amran, Y.H.M., Alyousef, R., Alabduljabbar, H., 2020. Renewable and sustainable energy production in Saudi Arabia according to Saudi vision 2030; current status and future prospects. J. Clean. Prod. 247, 119602 https://doi.org/10.1016/j.jclepro.2019.119602.

Axelsson, G., Stefánsson, V., Björnsson, G., Liu, J., 2005. Sustainable management of geothermal resources and utilization for 100–300 years. In: Proceedings of the World Geothermal Congress, International Geothermal Association. Antalya, Turkey, pp. 1–8, 24-29 April.

Battistelli, A., Calore, C., Pruess, K., 1997. The simulator TOUGH2/EWASG for modelling geothermal reservoirs with brines and non-condensible gas. Geothermics 26, 437–464. https://doi.org/10.1016/S0375-6505(97)00007-2.

Beckers, K.F., Kolker, A., Pauling, H., McTigue, J.D., Kesseli, D., 2021. Evaluating the feasibility of geothermal deep direct-use in the United States. Energy Convers. Manag. 243, 114335 https://doi.org/10.1016/j.enconman.2021.114335.

Beckers, K.F., McCabe, K., 2019. GEOPHIRES v2.0: updated geothermal techno-economic simulation tool. Geotherm. Energy 7. https://doi.org/10.1186/s40517-019-0119-6.

Bell, I.H., Jäger, A., 2016. Helmholtz energy transformations of common cubic equations of state for use with pure fluids and mixtures. J. Res. Natl. Inst. Stand. Technol. 121, 26. https://doi.org/10.6028/jres.121.011.

Bell, I.H., Wronski, J., Quoilin, S., Lemort, V., 2014. Pure and pseudo-pure fluid thermophysical property evaluation and the open-source thermophysical property

library CoolProp. Ind. Eng. Chem. Res. 53, 2498–2508. https://doi.org/10.1021/ie4033999.
Birdsell, D.T., Adams, B.M., Saar, M.O., 2021. Minimum transmissivity and optimal well spacing and flow rate for high-temperature aquifer thermal energy storage. Appl. Energy 289. https://doi.org/10.1016/j.apenergy.2021.116658.
Buijze, L., van Bijsterveldt, L., Cremer, H., Paap, B., Veldkamp, H., Wassing, B.B.T., van Wees, J.-D., van Yperen, G.C.N., ter Heege, J.H., Jaarsma, B., 2019. Review of induced seismicity in geothermal systems worldwide and implications for geothermal systems in the Netherlands. Neth. J. Geosci. 98, e13. https://doi.org/10.1017/njg.2019.6.
Bush, J., Siega, C., 2010. Big bore well drilling in New Zealand – a case study. In: Proceedings of the World Geothermal Congress. Bali, Indonesia, p. 7.
Byerlee, J., 1978. Friction of rocks. Pure Appl. Geophys. 116, 615–626. https://doi.org/10.1007/BF00876528.
Cole, G.A., Abu-Ali, M.A., Coiling, E.L., Halpern, H.I., Carrigan, W.J., Savage, G.R., Scolaro, R.J., Al-Sharidi, S.H., 1995. Petroleum geochemistry of the Midyan and Jaizan basins of the Red Sea, Saudi Arabia. Mar. Pet. Geol. 12, 597–614. https://doi.org/10.1016/0264-8172(95)98087-L.
Daniilidis, A., Alpsoy, B., Herber, R., 2017. Impact of technical and economic uncertainties on the economic performance of a deep geothermal heat system. Renew. Energy 114, 805–816. https://doi.org/10.1016/j.renene.2017.07.090.
Daniilidis, A., Saeid, S., Doonechaly, N.G., 2021. The fault plane as the main fluid pathway: geothermal field development options under subsurface and operational uncertainty. Renew. Energy 171, 927–946. https://doi.org/10.1016/j.renene.2021.02.148.
Dawoud, M.A., 2005. The role of desalination in augmentation of water supply in GCC countries. Desalination 186, 187–198. https://doi.org/10.1016/J.DESAL.2005.03.094.
DOE. Geothermal electricity technology evaluation model (GETEM) Department of energy (DOE). https://energy.gov/eere/geothermal/geothermal-electricity-technology-evaluation-model.
Dumas, P., Angelino, L., 2015. GeoDH: promote geothermal district heating systems in Europe. April 19–2. In: Proceedings of the World Geothermal Congress5. Melbourne, Australia. April 19–2.
ECRA, 2009. Saudi Arabia Electricity & Cogeneration Regulatory Authority (ECRA) Annual report: Activities and Achievements of the Authority in 2009. https://ext.ecra.gov.sa/en-us/MediaCenter/DocLib2/Lists/SubCategory_Library/4%20ECRA%20activities%20report%202009_webEnglish.pdf.
EIA, 2020. Saudi Arabia Used Less Crude Oil for Power Generation in 2018. The US Energy Information Administration (EIA). https://www.eia.gov/todayinenergy/detail.php?id=39693.
EIA, 2019. Nearly Half of U.S. Geothermal Power Capacity Came Online in 1980s. The US Energy Information Administration (EIA). https://www.eia.gov/todayinenergy/detail.php?id=42036.
English, J.M., 2012. Thermomechanical origin of regional fracture systems. Am. Assoc. Pet. Geol. Bull. 96, 1597–1625. https://doi.org/10.1306/01021211018.
Ezekiel, J., Adams, B.M., Saar, M.O., Ebigbo, A., 2022. Numerical analysis and optimization of the performance of CO_2-plume geothermal (CPG) production wells and implications for electric power generation. Geothermics 98, 102270. https://doi.org/10.1016/j.geothermics.2021.102270.
Ezekiel, J., Ebigbo, A., Adams, B.M., Saar, M.O., 2020. Combining natural gas recovery and CO_2-based geothermal energy extraction for electric power generation. Appl. Energy 269, 1–21. https://doi.org/10.1016/j.apenergy.2020.115012.
Ezekiel, J., Kumbhat, D., Ebigbo, A., Adams, B.M., Saar, M.O., 2021. Sensitivity of reservoir and operational parameters on the energy extraction performance of combined CO_2-EGR–CPG systems. Energies. https://doi.org/10.3390/en14196122.
Farnoosh, A., Lantz, F., Percebois, J., 2014. Electricity generation analyses in an oil-exporting country: transition to non-fossil fuel based power units in Saudi Arabia. Energy 69, 299–308. https://doi.org/10.1016/j.energy.2014.03.017.
GeoDH, 2015a. Geothermal District Heating Case Study: Pomarance, Italy. http://geodh.eu/project/pomarance/.
GeoDH, 2015b. Geothermal District Heating Case Study Podhale, Poland. http://geodh.eu/project/pomarance/.
GeoDH, 2015c. Geothermal District Heating Case Study Lendava, Slovenia. http://geodh.eu/project/lendava/.
Girdler, R.W., 1970. A review of red sea heat flow. Philos. Trans. R. Soc. Lond. Ser. A Math. Phys. Sci. 267, 191–203.
Girdler, R.W., Evans, T.R., 1977. Red Sea heat flow. Geophys. J. Int. 51, 245–251. https://doi.org/10.1111/j.1365-246X.1977.tb04199.x.
Huang, T.Y., Pérez-Cardona, J.R., Zhao, F., Sutherland, J.W., Paranthaman, M.P., 2021. Life cycle assessment and techno-economic assessment of lithium recovery from geothermal brine. ACS Sustain. Chem. Eng. 9, 6551–6560. https://doi.org/10.1021/acssuschemeng.0c08733.
Hughes, G.W., Johnson, R.S., 2005. Lithostratigraphy of the Red sea region. GeoArabia 10, 49–126. https://doi.org/10.2113/geoarabia100349.
IEA, 2018. International energy agency (IEA). World Energy Outlook 2018. IEA. https://doi.org/10.1787/weo-2018-2-en.
IEA Geothermal, 2017. 2016 Annual Report. The International Energy Agency (IEA) Geothermal.
IPCC, 2012. Intergovernmental Panel on Climate Change (IPCC) Special Report on Renewable Energy Sources and Climate Change Mitigation. Chapter 9: Renewable Energy in the Context of Sustainable Development. https://archive.ipcc.ch/pdf/special-reports/srren/drafts/Chapter%2009%20SOD.pdf.
Ke, T., Huang, S., Xu, W., Tang, X., Li, X., 2022. Evaluation of the multi-doublet performance in sandstone reservoirs using thermal-hydraulic modeling and economic analysis. Geothermics 98, 102273. https://doi.org/10.1016/j.geothermics.2021.102273.
Kralj, P., 2005. Geothermal project benedikt: possibilities for geothermal energy use in small communities. In: Proceedings of the World Geothermal Congress. Antalya, Turkey. April 24–29.
Lashin, A., Al Arifi, N., 2014. Geothermal energy potential of southwestern of Saudi Arabia "exploration and possible power generation": a case study at Al Khouba area – Jizan. Renew. Sustain. Energy Rev. 30, 771–789. https://doi.org/10.1016/j.rser.2013.10.037.
Lashin, A., Al Arifi, N., 2012. The geothermal potential of Jizan area, southwestern parts of Saudi Arabia. Int. J. Phys. Sci. 7, 664–675.
Le Quéré, C., Jackson, R.B., Jones, M.W., Smith, A.J.P., Abernethy, S., Andrew, R.M., De-Gol, A.J., Willis, D.R., Shan, Y., Canadell, J.G., Friedlingstein, P., Creutzig, F., Peters, G.P., 2020. Temporary reduction in daily global CO_2 emissions during the COVID-19 forced confinement. Nat. Clim. Chang. 10, 647–653. https://doi.org/10.1038/s41558-020-0797-x.
Limberger, J., Boxem, T., Pluymaekers, M., Bruhn, D., Manzella, A., Calcagno, P., Beekman, F., Cloetingh, S., van Wees, J.D., 2018. Geothermal energy in deep aquifers: a global assessment of the resource base for direct heat utilization. Renew. Sustain. Energy Rev. https://doi.org/10.1016/j.rser.2017.09.084.
Liu, Z., Deng, Z., Davis, S.J., Giron, C., Ciais, P., 2022. Monitoring global carbon emissions in 2021. Nat. Rev. Earth Environ. https://doi.org/10.1038/s43017-022-00285-w.
Lu, S.M., 2018. A global review of enhanced geothermal system (EGS). Renew. Sustain. Energy Rev. https://doi.org/10.1016/j.rser.2017.06.097.
Lucazeau, F., 2019. Analysis and mapping of an updated terrestrial heat flow data set. Geochem. Geophys. Geosyst. 20, 4001–4024. https://doi.org/10.1029/2019GC008389.
Lukawski, M.Z., Anderson, B.J., Augustine, C., Capuano, L.E., Beckers, K.F., Livesay, B., Tester, J.W., 2014. Cost analysis of oil, gas, and geothermal well drilling. J. Pet. Sci. Eng. 118, 1–14. https://doi.org/10.1016/j.petrol.2014.03.012.
Lund, J.W., Toth, A.N., 2021. Direct utilization of geothermal energy 2020 worldwide review. Geothermics 90, 101915. https://doi.org/10.1016/j.geothermics.2020.101915.
Majer, E.L., Baria, R., Stark, M., Oates, S., Bommer, J., Smith, B., Asanuma, H., 2007. Induced seismicity associated with enhanced geothermal systems. Geothermics 36, 185–222. https://doi.org/10.1016/j.geothermics.2007.03.003.
McCabe, K., Beckers, K., Young, K.R., Blair, N., 2019. GeoVision Analysis Supporting Task Force Report: Thermal Applications—Quantifying Technical, Economic, and Market Potential of Geothermal District Heating Systems in the United States. National Renewable Energy Laboratory, Golden, CO. NREL/TP-6A20-71715.
Menon, E.S., 2011. Chapter 9 - Series and Parallel Piping and Power Required. Pipeline Planning and Construction Field Manual. Gulf Professional Publishing, Boston, pp. 177–204. https://www.sciencedirect.com/science/article/pii/B9780123838674000098.
Nada, N., 2013. Desalination in Saudi Arabia: an overview. In: Proceedings of the Saudi Arabian Water Environment Association (SAWEA) Conference: Water Arabia.
Petursson, B., 2015. Renewable energy in iceland: with focus on geothermal district heating. In: Proceedings of the EU-Eastern Partnership STI Cooperation: Energy Research and Innovation, Minsk. October 12–13.
Pollack, H.N., Hurter, S.J., Johnson, J.R., 1993. Heat flow from the Earth's interior: analysis of the global data set. Rev. Geophys. 31, 267–280. https://doi.org/10.1029/93RG01249.
Pruess, K., 2008. On production behavior of enhanced geothermal systems with CO_2 as working fluid. Energy Convers. Manag. 49, 1446–1454. https://doi.org/10.1016/j.enconman.2007.12.029.
Pruess, K., 2006. Enhanced geothermal systems (EGS) using CO_2 as working fluid-A novel approach for generating renewable energy with simultaneous sequestration of carbon. Geothermics 35, 351–367. https://doi.org/10.1016/j.geothermics.2006.08.002.
CoolProp, 2019. CoolProp 6.2.1 documentation (MATLAB Wrapper). http://www.coolprop.org/coolprop/wrappers/MATLAB/index.html.
Pruess, K., Oldenburg, C., Moridis, G., 2012. TOUGH2 user's guide, version 2 (revised). https://tough.lbl.gov/assets/docs/TOUGH2_V2_Users_Guide.pdf.
Randolph, J.B., Saar, M.O., 2011. Combining geothermal energy capture with geologic carbon dioxide sequestration. Geophys. Res. Lett. 38, 1–7. https://doi.org/10.1029/2011GL047265.
Reber, T.J., 2013. Evaluating Opportunities for Enhanced Geothermal System-Based District Heating in New York and Pennsylvania. Cornell University, Ithaca, New York, United States. MS thesis.
Rolandone, F., Lucazeau, F., Leroy, S., Mareschal, J.-C., Jorand, R., Goutorbe, B., Bouquerel, H., 2013. New heat flow measurements in Oman and the thermal state of the Arabian shield and platform. Tectonophysics 589, 77–89. https://doi.org/10.1016/j.tecto.2012.12.034.
Rybach, L., 2003. Geothermal energy: sustainability and the environment. Geothermics 32, 463–470. https://doi.org/10.1016/S0375-6505(03)00057-9.
Salam, M.A., Khan, S.A., 2018. Transition towards sustainable energy production – a review of the progress for solar energy in Saudi Arabia. Energy Explor. Exploit. 36, 3–27. https://doi.org/10.1177/0144598717737442.
Sanjuan, B., Millot, R., Innocent, C., Dezayes, C., Scheiber, J., Brach, M., 2016. Major geochemical characteristics of geothermal brines from the Upper Rhine Graben granitic basement with constraints on temperature and circulation. Chem. Geol. 428, 27–47. https://doi.org/10.1016/j.chemgeo.2016.02.021.
Services, CFG, Ross Offshore. Towards the Industrialisation of Geothermal Energy in Denmark: A look at 35 Years of Success in Geothermal Energy for District Heating in

France. http://www.energy-cities.eu/IMG/pdf/st_denmark_cfg_services_and_ross_offshore_09.14.2016.pdf.
Tester, J.W., Beckers, K.F., Hawkins, A.J., Lukawski, M.Z., 2021. The evolving role of geothermal energy for decarbonizing the United States. Energy Environ. Sci. 14, 6211–6241. https://doi.org/10.1039/D1EE02309H.
Thorsteinsson, H.H., Tester, J.W., 2010. Barriers and enablers to geothermal district heating system development in the United States. Energy Policy 38, 803–813. https://doi.org/10.1016/j.enpol.2009.10.025.
Ungemach, P., 2012. Geothermal: insight into geothermal technology. In: Proceedings of the Annual Conference Teaming up for Renewable Heating and Cooling. Copenhagen, Denmark. April 26–27.
Watanabe, H., Yamada, N., Okaji, M., 2004. Linear thermal expansion coefficient of silicon from 293 to 1000 K. Int. J. Thermophys. 25, 221–236. https://doi.org/10.1023/B:IJOT.0000022336.83719.43.
World Nuclear Association (WNA), 2011. Comparison of Lifecycle Greenhouse Gas Emissions of Various Electricity Generation Sources. World Nuclear Association (WNA).
Xu, C., Dowd, P.A., Tian, Z.F., 2015. A simplified coupled hydro-thermal model for enhanced geothermal systems. Appl. Energy 140, 135–145. https://doi.org/10.1016/j.apenergy.2014.11.050.
Zaal, C., Daniilidis, A., Vossepoel, F.C., 2021. Economic and fault stability analysis of geothermal field development in direct-use hydrothermal reservoirs. Geotherm. Energy 9, 12. https://doi.org/10.1186/s40517-021-00193-0.
Zhang, L., Ezekiel, J., Li, D., Pei, J., Ren, S., 2014a. Potential assessment of CO_2 injection for heat mining and geological storage in geothermal reservoirs of China. Appl. Energy 122, 237–246. https://doi.org/10.1016/j.apenergy.2014.02.027.
Zhang, Y.-J., Li, Z.-W., Guo, L.-L., Gao, P., Jin, X.-P., Xu, T.-F., 2014b. Electricity generation from enhanced geothermal systems by oilfield produced water circulating through reservoir stimulated by staged fracturing technology for horizontal wells: a case study in Xujiaweizi area in Daqing Oilfield, China. Energy 78, 788–805. https://doi.org/10.1016/j.energy.2014.10.073.
Zoback, M.D., Barton, C.A., Brudy, M., Castillo, D.A., Finkbeiner, T., Grollimund, B.R., Moos, D.B., Peska, P., Ward, C.D., Wiprut, D.J., 2003. Determination of stress orientation and magnitude in deep wells. Int. J. Rock Mech. Min. Sci. 40, 1049–1076. https://doi.org/10.1016/j.ijrmms.2003.07.001.